Secondary Organic Aerosol (SOA) yields from NO_3 radical + isoprene based on nighttime aircraft power plant plume transects

Juliane L. Fry[1], Steven S. Brown[2,5], Ann M. Middlebrook[2], Peter M. Edwards[2,3,4], Pedro Campuzano-Jost[3,5], Douglas A. Day[3,5], José L. Jimenez[3,5], Hannah M. Allen[6], Thomas B. Ryerson[2], Ilana Pollack[2,3,a], Martin Graus[3,b], Carsten Warneke[2.3], Joost A. deGouw[3,5], Charles A. Brock[2], Jessica Gilman[2,3], Brian M. Lerner[2,3,c], William P. Dubé[2,3], Jin Liao[2,3,d], André Welti[2,3,e]

[1]Chemistry Department, Reed College, Portland, OR, USA
[2]Chemical Sciences Division, Earth System Research Laboratory, National Oceanic and Atmospheric Administration, Boulder, CO, USA
[3]Cooperative Institute for Research in Environmental Sciences, University of Colorado, Boulder, CO, USA
[4]Wolfson Atmospheric Chemistry Laboratories, Department of Chemistry, University of York, York, UK
[5]Department of Chemistry, University of Colorado, Boulder, CO, USA
[6]Division of Chemistry and Chemical Engineering, California Institute of Technology, Pasadena, CA, USA
[a]now at Department of Atmospheric Science, Colorado State University, Fort Collins, CO, USA
[b]now at Department of Atmospheric and Cryospheric Sciences, University of Innsbruck, Austria.
[c]now at Aerodyne Research, Inc., Billerica, MA, USA
[d]now at Universities Space Research Association, Columbia, MD, USA and NASA Goddard Space Flight Center, Atmospheric Chemistry and Dynamic Laboratory, Greenbelt, MD, USA
[e]now at Leibniz Institute for Tropospheric Research, Department of Physics, Leipzig, Germany

Abstract

Nighttime reaction of nitrate radicals (NO_3) with biogenic volatile organic compounds (BVOC) has been proposed as a potentially important but also highly uncertain source of secondary organic aerosol (SOA). The southeast United States has both high BVOC and nitrogen oxide (NO_x) emissions, resulting in a large model-predicted NO_3-BVOC source of SOA. Coal-fired power plants in this region constitute substantial NO_x emissions point sources into a nighttime atmosphere characterized by high regionally widespread concentrations of isoprene. In this paper, we exploit nighttime aircraft observations of these power plant plumes, in which NO_3 radicals rapidly remove isoprene, to obtain field-based estimates of the secondary organic aerosol yield from NO_3 + isoprene. Observed in-plume increases in nitrate aerosol are consistent with organic nitrate aerosol production from NO_3 + isoprene, and these are used to determine molar SOA yields, for which the average over 9 plumes is 9% (+/- 5%). Corresponding mass yields depend on the assumed molecular formula for isoprene-NO_3-SOA, but the average over 9 plumes is 27% (+/- 14%), on average larger than those previously measured in chamber studies (12 – 14% mass yield as ΔOA/ΔVOC after oxidation of both double bonds). Yields are larger for longer plume ages. This suggests that ambient aging processes lead more effectively to condensable material than typical chamber conditions allow. We discuss potential mechanistic explanations for this difference, including longer ambient peroxy radical lifetimes and heterogeneous reactions of NO_3-isoprene gas phase products.

More in-depth studies are needed to better understand the aerosol yield and oxidation mechanism of NO_3 radical + isoprene, a coupled anthropogenic – biogenic source of SOA that may be regionally significant.

1 Introduction

Organic aerosol (OA) is increasingly recognized as a globally important component of the fine particulate matter that exerts a large but uncertain negative radiative forcing on Earth's climate (Myhre et al., 2013) and adversely affects human health around the world (Lelieveld et al., 2015).This global importance is complicated by large regional differences in OA concentrations relative to other sources of aerosol such as black carbon, sulfate, nitrate and sea salt. OA comprises 20 – 50% of total fine aerosol mass at continental mid-latitudes, but more in urban environments and biomass burning plumes, and up to 90% over tropical forests (Kanakidou et al., 2005;Zhang et al., 2007). Outside of urban centers and fresh biomass burning plumes, the majority of this OA is secondary organic aerosol (SOA) (Jimenez et al., 2009), produced by oxidation of directly emitted volatile organic compounds followed by partitioning into the aerosol phase. Forests are strong biogenic VOC emitters, in the form of isoprene (C_5H_8), monoterpenes ($C_{10}H_{16}$), and sesquiterpenes ($C_{15}H_{24}$), all of which are readily oxidized by the three major atmospheric oxidants, OH, NO_3, and O_3. The total global source of biogenic SOA from such reactions remains highly uncertain, with a eview estimating it at 90 +/- 90 Tg C yr^{-1} (Hallquist et al., 2009), a large fraction of which may be anthropogenically controlled (Spracklen et al., 2011;Goldstein et al., 2009;Carlton et al., 2010;Hoyle et al., 2011). As most NO_3 arises from anthropogenic emissions, OA production from NO_3 + isoprene is one mechanism that could allow for the anthropogenic control of biogenic SOA mass loading.

Isoprene constitutes nearly half of all global VOC emissions to the atmosphere, with a flux of ~600 Tg yr^{-1} (Guenther et al., 2006). As a result, accurate global biogenic SOA budgets depend strongly on yields from isoprene oxidation. Recent global modeling efforts find that isoprene SOA is produced at rates from 14 (Henze and Seinfeld, 2006;Hoyle et al., 2007) to 19 TgC yr^{-1} (Heald et al., 2008), which implies that it could constitute 27% (Hoyle et al., 2007) to 48% (Henze and Seinfeld, 2006) to 78% (Heald et al., 2008) of total SOA (based also on varying estimates of total SOA burden in each study). More recent observational constraints on SOA yield from isoprene find complex temperature-dependent mechanisms that could affect vertical distributions (Worton et al., 2013) and suggest that isoprene SOA constitutes from 17% (Hu et al., 2015) to 40% (Kim et al., 2015) up to 48% (Marais et al., 2016) of total OA in the southeastern United States. This large significance comes despite isoprene's low SOA mass yields – two recent observational studies estimated the total isoprene SOA mass yield to be ~3% (Marais et al., 2016;Kim et al., 2015), and modeling studies typically estimate isoprene SOA yields to be 4 to 10%, depending on the oxidant, in contrast to monoterpenes' yields of 10 to 20% and sesquiterpenes' yields of >40% (Pye et al., 2010). Furthermore, laboratory studies of SOA mass yields may have a tendency to underestimate these yields, if they cannot access the longer timescales of later-generation chemistry, or are otherwise run under conditions that limit oxidative aging of first-generation products (Carlton et al., 2009).

Laboratory chamber studies of SOA mass yield at OA loadings of ~ 10 μg m^{-3} from isoprene have typically found low yields from O_3 (1% (Kleindienst et al., 2007)) and OH (2% at low NO_x to 5% at high NO_x (Kroll et al., 2006;Dommen et al., 2009); 1.3% at low NO_x and neutral seed aerosol pH but rising to 29% in the presence of acidic sulfate seed aerosol due to reactive uptake of epoxydiols of isoprene (IEPOX) (Surratt et al., 2010)). One recent chamber study on OH-initiated isoprene SOA formation focused on the fate of second-generation RO_2 radical found significantly higher yields, up to 15% at low NO_x (Liu et al., 2016), suggesting that omitting later-generation oxidation chemistry could be an important limitation of early chamber determinations of isoprene SOA yields. Another found an increase in SOA formed with increasing HO_2 to RO_2 ratios, suggesting that RO_2 fate could also play a role in the variability of previously reported SOA yields (D'Ambro et al., 2017).

For NO_3 oxidation of isoprene, early chamber experiments already pointed to higher yields (e.g., 12% (Ng et al., 2008)) than for OH oxidation. Ng et al. (Ng et al., 2008) also observed chemical regime differences: SOA yields were approximately two times larger when chamber conditions were tuned such that first-generation peroxy radical fate was RO_2+RO_2 dominated than when it was RO_2+NO_3 dominated. In addition, Rollins et al. (Rollins et al., 2009) observed a significantly higher SOA yield (14%) from second-generation NO_3 oxidation than that when only one double bond was oxidized (0.7%). This points to the possibility that later-generation, RO_2+RO_2 dominated isoprene + NO_3 chemistry may be an even more substantial source of SOA than what current chamber studies have captured. Schwantes et al. (Schwantes et al., 2015) investigated the gas-phase products of NO_3 + isoprene in the RO_2+HO_2 dominated regime and found the major product to be isoprene nitrooxy hydroperoxide (INP, 75-78% molar yield), which can photochemically convert to isoprene nitrooxy hydroxyepoxide (INHE), a molecule that might contribute to SOA formation via heterogeneous uptake similar to IEPOX. Here again, multiple generations of chemistry are required to produce products that may contribute to SOA.

Because the SOA yield appears to be highest for NO_3 radical oxidation, and isoprene is such an abundantly emitted BVOC, oxidation of isoprene by NO_3 may be an important source of OA in areas with regional NO_x pollution. Since the SOA yield with neutral aerosol seed appears to be an order of magnitude larger than that from other oxidants, even if only 10% of isoprene is oxidized by NO_3, it will produce comparable SOA to daytime photo-oxidation. For example, Brown et al. (Brown et al., 2009) concluded that NO_3 contributed more SOA from isoprene than OH over New England, where > 20% of isoprene emitted during the previous day was available at sunset to undergo dark oxidation by either NO_3 or O_3. The corresponding contribution to total SOA mass loading was 1 – 17% based on laboratory yields (Ng et al., 2017). Rollins et al. (Rollins et al., 2012) concluded that multi-generational NO_3 oxidation of biogenic precursors was responsible for one-third of nighttime organic aerosol increases during the CalNex-2010 experiment in Bakersfield, CA. In an aircraft study near Houston, TX, Brown et al. (Brown et al., 2013) observed elevated organic aerosol in the nighttime boundary layer, and correlated vertical profiles of organic and nitrate aerosol in regions with rapid surface level NO_3 radical production and BVOC emissions. From these observations, the authors estimated an SOA source from NO_3 + BVOCs within the nocturnal boundary layer of 0.05 – 1 μg m^{-3} h^{-1}. Carlton et al. (Carlton et al., 2009) note the large scatter in chamber-measured SOA yields from isoprene

photooxidation and point throughout their review of SOA formation from isoprene to the likely importance of poorly understood later generations of chemistry in explaining field observations. We suggest that similar differences in multi-generational chemistry could explain the variation among the (sparse) chamber and field observations of NO_3 + isoprene yields described in the previous paragraph, and summarized in a recent review of NO_3 + BVOC oxidation mechanisms and SOA formation (Ng et al., 2017).

The initial products of NO_3 + isoprene include organic nitrates, some of which will partially partition to the aerosol phase. Organic nitrates in the particle phase ($pRONO_2$) are challenging to quantify with online methods, due to both interferences and their often overall low concentrations in ambient aerosol. Hence, field datasets to constrain modeled $pRONO_2$ are sparse (Ng et al., 2017;Fisher et al., 2016). One of the most used methods in recent studies, used also here, is quantification with the Aerodyne Aerosol Mass Spectrometer (AMS). Organic nitrates thermally decompose in the AMS vaporizer and different approaches have been used to apportion the organic fraction contributing to the total nitrate signal. Allan et al. (Allan et al., 2004a) first proposed the use of nitrate peaks at *m/z* 30 and 46 to distinguish various nitrate species with the AMS. Marcolli et al. (Marcolli et al., 2006), in the first reported tentative assignment of aerosol organic nitrate using AMS data, used cluster analysis to analyze data from the 2002 New England Air Quality Study. In that study, cluster analysis identified two categories with high *m/z* 30 contributions. One of these peaked in the morning when NO_x was abundant and was more prevalent in plumes with lowest photochemical ages, potentially from isoprene oxidation products. The second was observed throughout the diurnal cycle in both fresh and aged plumes, and contained substantial *m/z* 44 contribution (highly oxidized OA). A subsequent AMS laboratory and field study discussed and further developed methods for separate quantification of organic nitrate (in contrast to inorganic nitrate) (Farmer et al., 2010). A refined version of one of these separation methods, based on the differing NO_2^+/NO^+ fragmentation ratio for organic vs. inorganic nitrate, was later employed to quantify organic nitrate aerosol at two forested rural field sites where strong biogenic VOC emissions and relatively low NOx combined to make substantial organic nitrate aerosol concentrations ((Fry et al., 2013;Ayres et al., 2015)). Most recently, Kiendler-Scharr et al. (Kiendler-Scharr et al., 2016) used a variant of this method to conclude that across Europe, organic nitrates comprise ~40% of submicron organic aerosol. Modeling analysis concluded that a substantial fraction of this organic nitrate aerosol is produced via NO_3 radical initiated chemistry. Chamber studies have employed this fragmentation ratio method to quantify organic nitrates (Boyd et al., 2015;Bruns et al., 2010;Fry et al., 2009;Fry et al., 2011;Rollins et al., 2009), providing the beginnings of a database of typical organonitrate fragmentation ratios from various BVOC precursors.

Measurements conducted at the SOAS ground site in Centreville, Alabama in 2013 found evidence of significant organonitrate contribution to SOA mass loading. Xu et al. (Xu et al., 2015) reported that organic nitrates constituted 5 to 12% of total organic aerosol mass from AMS data applying a variant of the NO_2^+/NO^+ ratio method. They identify a nighttime-peaking "LO-OOA" AMS factor which they attribute to mostly NO_3 oxidation of BVOC (in addition to O_3 + BVOC). They estimated that the NO_3 radical oxidizes 17% of isoprene, 20% of α-pinene, and 38% of β-pinene in the nocturnal boundary layer at this site. However, applying laboratory-

based SOA yields to model the predicted increase in OA, Xu et al. predict only 0.7 μg m^{-3} of SOA would be produced, substantially lower than the measured nighttime LO-OOA production of 1.7 μg m^{-3}. The more recent analysis of Zhang et al. (Zhang et al., 2018) found a strong correlation of monoterpene SOA with the fraction of monoterpene oxidation attributed to NO_3, even for non-nitrate containing aerosol, suggesting an influence of NO_3 even in pathways that ultimately eliminate the nitrate functionality from the SOA, such as hydrolysis or NO_2 regeneration. Ayres et al. (Ayres et al., 2015) used a correlation of overnight organonitrate aerosol buildup with calculated net NO_3 + monoterpene and isoprene reactions to estimate an overall NO_3 + monoterpene SOA mass yield of 40 – 80%. The factor of two range in this analysis was based on two different measurements of aerosol-phase organic nitrates. These authors used similar correlations to identify specific CIMS-derived molecular formulae that are likely to be NO_3 radical chemistry products of isoprene and monoterpenes, and found minimal contribution of identified first-generation NO_3 + isoprene products to the aerosol phase (as expected based on their volatility). Lee et al. (Lee et al., 2016) detected abundant highly functionalized particle-phase organic nitrates at the same site, with apparent origin both from isoprene and monoterpenes, and both daytime and nighttime oxidation, and estimated their average contribution to submicron organic aerosol mass to be between 3 – 8 %. For the same ground campaign, Romer et al. (Romer et al., 2016) found evidence of rapid conversion from alkyl nitrates to HNO_3, with total alkyl nitrates having an average daytime lifetime of 1.7 hours.

Xie et al. (Xie et al., 2013) used a model constrained by observed alkyl nitrate correlations with O_3 from the INTEX-NA/ICARTT 2004 field campaign to determine a range of isoprene nitrate lifetimes between 4 and 6 hours, with 40-50% of isoprene nitrates formed by NO_3 + isoprene reactions. Laboratory studies show that not all organic nitrates hydrolyze to HNO_3 equally rapidly: primary and secondary organic nitrates were found to be less prone to aqueous hydrolysis than tertiary organic nitrates (Darer et al., 2011;Hu et al., 2011;Fisher et al., 2016;Boyd et al., 2015). This suggests that field-based estimates of the contribution of organic nitrates to SOA formation could be a lower limit, if they are based on measurement of those aerosol-phase nitrates. This is because if hydrolysis is rapid, releasing HNO_3 but leaving behind the organic fraction in the aerosol phase, then that organic mass would not be accurately accounted for as arising from nitrate chemistry. This was addressed in a recent modeling study of SOAS (Pye et al., 2015) in which modeled hydrolysis products of particulate organic nitrates of up to 0.8 μg m^{-3} additional aerosol mass loading in the southeast U.S. were included in the estimate of change in OA due to changes in NO_x. Another recent GEOS-Chem modeling study using of gas- and particle-phase organic nitrates observed during the SEAC^{4}RS and SOAS campaigns similarly finds $RONO_2$ to be a major sink of NO_x across the SEUS region (Fisher et al., 2016;Lee et al., 2016).

Complementing these SOAS ground site measurements, the NOAA-led SENEX (Southeast Nexus) aircraft campaign conducted 18 research flights focused in part on studying the interactions between biogenic and anthropogenic emissions that form secondary pollutants between 3 June and 10 July 2013 (Warneke et al., 2016). Flight instrumentation focused on measurement of aerosol precursors and composition enable the present investigation of SOA yields using this aircraft data set. Edwards et al. (Edwards et al., 2017) used data from the

SENEX night flights to evaluate the nighttime oxidation of BVOC, observing high nighttime isoprene mixing ratios in the residual layer that can undergo rapid NO_3 oxidation when sufficient NO_x is present. These authors suggest that past NO_x reductions may have been uncoupled from OA trends due to NO_x not having been the limiting chemical species for OA production, but that future reductions in NO_x may decrease OA if NO_3 oxidation of BVOC is a substantial regional SOA source. Because isoprene is ubiquitous in the nighttime residual layer over the southeastern United States and the NO_3 + isoprene reaction is rapid, NO_3 reaction will be dominant relative to O_3 in places with anthropogenic inputs of NO_x (Edwards et al. (Edwards et al., 2017) concludes that when NO_2/BVOC > 0.5, NO_3 oxidation will be dominant). Hence, a modest NO_3 + isoprene SOA yield may constitute a regionally important OA source.

Several modeling studies have investigated the effects of changing NO_x on global and SEUS SOA. Hoyle et al. (Hoyle et al., 2007) found an increase in global SOA production from 35 Tg yr^{-1} to 53 Tg yr^{-1} since preindustrial times, resulting in an increase in global annual mean SOA mass loading of 51%, attributable in part to changing NO_x emissions. Zheng et al. (Zheng et al., 2015) found only moderate SOA reductions from a 50% reduction in NO emissions: 0.9 – 5.6 % for global NO_x or 6.4 – 12.0% for southeast US NO_x, which they attributed to buffering by alternate chemical pathways and offsetting tendencies in the biogenic vs. anthropogenic SOA components. In contrast, Pye et al. (Pye et al., 2015) find a 9% reduction in total organic aerosol in Centreville, AL for only 25% reduction in NO_x emissions. A simple limiting-reagent analysis of NO_3 + monoterpene SOA from power plant plumes across the United States found that between 2008 and 2011, based on EPA-reported NO_x emissions inventories, some American power plants shifted to the NO_x-limited regime (from 3.5% to 11% of the power plants), and showed that these newly NO_x-limited power plants were primarily in the southeastern United States (Fry et al., 2015). The effect of changing NO_x on SOA burden is clearly still in need of further study.

Here, we present aircraft transects of spatially discrete NO_x plumes from electric generating units (EGU), or power plants (PP), as a method to specifically isolate the influence of NO_3 oxidation. These plumes are concentrated and highly enriched in NO_x over a scale of only a few km (Brown et al., 2012), and have nitrate radical production rates ($P(NO_3)$) 10 – 100 times greater than those of background air. The rapid shift in $P(NO_3)$ allows direct comparison of air masses with slow and rapid oxidation rates attributable to the nitrate radical, effectively isolating the influence of this single chemical pathway in producing SOA and other oxidation products. Changes in organic nitrate aerosol ($pRONO_2$) concentration and accompanying isoprene titration enable a direct field determination of the SOA yield from NO_3 + isoprene.

2 Field campaign and experimental and modeling methods

The Southeast Nexus (SENEX: http://esrl.noaa.gov/csd/projects/senex/) campaign took place 3 June through 10 July 2013 as the NOAA WP-3D aircraft contribution to the larger Southeast Atmospheric Study (SAS: http://www.eol.ucar.edu/field_projects/sas/), a large, coordinated research effort focused on understanding natural and anthropogenic emissions, oxidation chemistry and production of aerosol in the summertime atmosphere in the southeastern United States. The NOAA WP-3D aircraft operated 18 research flights out of Smyrna, Tennessee,

carrying an instrument payload oriented towards elucidating emissions inventories and reactions of atmospheric trace gases, and aerosol composition and optical properties (Warneke et al., 2016). One of the major goals of the larger SAS study is to quantify the fraction of organic aerosol that is anthropogenically controlled, with a particular focus on understanding how OA may change in the future in response to changing anthropogenic emissions.

The subset of aircraft instrumentation employed for the present analysis of nighttime NO_3 + isoprene initiated SOA production includes measurements used to determine NO_3 radical production rate ($P(NO_3) = k_{NO2+O3}(T)\,[NO_2]\,[O_3]$), isoprene and monoterpene concentrations, other trace gases for plume screening and identification, aerosol size distributions, and aerosol composition. The details on the individual measurements and the overall aircraft deployment goals and strategy are described in Warneke et al. (Warneke et al., 2016). Briefly, NO_2 was measured by UV photolysis and gas-phase chemiluminescence (P-CL) and by cavity ringdown spectroscopy, (CRDS), which agreed within 6%. O_3 was also measured by both gas-phase chemiluminescence and CRDS and agreed within 8%, within the combined measurement uncertainties of the instruments. Various volatile organic compounds were measured with several techniques, including for the isoprene and monoterpenes of interest here, proton reaction transfer mass spectrometry (PTR-MS) and canister whole air samples and post-flight GC-MS analysis (iWAS/GCMS). A comparison of PTR-MS and iWAS/GCMS measurements of isoprene during SENEX has high scatter due to imperfect time alignment and isoprene's high variability in the boundary layer, but the slope of the intercomparison is 1.04 ((Warneke et al., 2016); for more details on the VOC intercomparisons, see also Lerner et al., (Lerner et al., 2017)). Acetonitrile from the PTRMS was used to screen for the influence of biomass burning. Sulfur dioxide (SO_2) was used to identify emissions from coal-fired power plants. All gas-phase instruments used dedicated inlets, described in detail in the supplemental information for Warneke et al. (Warneke et al., 2016).

Aerosol particles were sampled downstream of a low turbulence inlet (Wilson et al., 2004), after which they were dried by ram heating, size-selected by an impactor with 1 μm aerodynamic diameter size cut-off, and measured by various aerosol instruments (Warneke et al., 2016). An ultra-high-sensitivity aerosol sizing spectrometer (UHSAS, Particle Metrics, Inc., Boulder, CO (Brock et al., 2011;Cai et al., 2008)) was used to measure the dry submicron aerosol size distribution down to about 70 nm. Data for the UHSAS are reported at 1 Hz whereas AMS data were recorded roughly every 10 seconds. The ambient (wet) surface areas were calculated according to the procedures described in Brock et al., 2016 (Brock et al., 2016). A pressure-controlled inlet (Bahreini et al., 2008) was employed to ensure that a constant mass flow rate was sampled by a compact time-of-flight aerosol mass spectrometer (C-ToF-AMS) which measured the non-refractory aerosol composition (Drewnick et al., 2005). The aerosol volume transmitted into the AMS was calculated by applying the measured AMS lens transmission curve (Bahreini et al., 2008) to the measured particle volume distributions from the UHSAS. For the entire SENEX study, the mean, calculated fraction of aerosol volume behind the 1 micron impactor that was transmitted through the lens into the AMS instrument was 97% (with ±4% standard deviation), indicating that most of the submicron aerosol volume measured by the sizing instruments was sampled by the AMS.

After applying calibrations and the composition-dependent collection efficiency following Middlebrook et al. (Middlebrook et al., 2012), the limits of detection for the flight analyzed here were 0.05 μg m^{-3} for nitrate, 0.26 μg m^{-3} for organic mass, 0.21 μg m^{-3} for ammonium, and 0.05 μg m^{-3} for sulfate, determined as three times the standard deviation of 10-second filtered air measurements obtained for 10 minutes during preflight and 10 minutes during postflight (110 datapoints). Note that the relative ionization efficiency for ammonium was 3.91 and 3.87 for the two bracketing calibrations and an average value of 3.9 was used for the flight analyzed here. An orthogonal distance regression (ODR-2) of the volume from composition data (AMS mass plus refractory black carbon) using a mass weighted density as described by Bahreini et al. (Bahreini et al., 2009) versus the volume based on the sizing instruments (after correcting for AMS lens transmission as above) had a slope of 1.06 for the entire SENEX study and 72% of the data points were within the measurements' combined uncertainties of ±45% (Bahreini et al., 2008). For the flight analyzed here, however, the same regression slope was 1.58, which is slightly higher than the combined uncertainties. It is unclear why the two types of volume measurements disagree more for this flight. This does not change the conclusions of this work because this has been incorporated into the error in aerosol organic nitrate, which still show positive enhancements in pRONO2 for these plumes (see Figure 4 below). These complete error estimates are also used in Figure 5 to clearly show the uncertainties in the yields. The volume comparison is discussed further in the Supplemental Information and shown for the plumes of interest in Fig. S1.

The C-ToF-AMS is a unit mass resolution (UMR) instrument and the mass spectral signals that are characteristic of aerosol nitrate at *m/z* 30 and 46 (NO^+ and NO_2^+) often contain interferences from organic species such as CH_2O^+ and $CH_2O_2^+$, respectively. Here, the *m/z* 30 and 46 signals have been corrected for these interferences by using correlated organic signals at *m/z* 29, 42, 43, and 45 that were derived from high-resolution AMS measurements during the NASA $SEAC^4RS$ campaign that took place in the same regions of the SE US shortly after SENEX (see Supplemental Information and Fig. S2). The corrections were applied to the individual flight analyzed here from July 2. All of the corrections were well correlated with each other for the $SEAC^4RS$ dataset and we used the organic peak at *m/z* 29 (from CHO^+) and the peak at *m/z* 45 (from CHO_2^+), respectively, since those corrections were from peaks closest (in *m/z*) to those being corrected. Once corrected, the nitrate mass concentrations in the final data archive for this flight were reduced by 0-0.24 μg sm^{-3}, an average reduction of 0.11 μg sm^{-3} or 32% from the initial nitrate mass concentrations. The organic interferences removed from the *m/z* 30 and *m/z* 46 signals are linearly correlated with the total organic mass concentrations, corresponding to an average 1.3% increase in the total organic mass.

The ratio of the corrected NO_2^+/NO^+ signals was then used to calculate the fraction of aerosol nitrate that was organic ($pRONO_2$) or inorganic (ammonium nitrate) based on the method described first in (Fry et al., 2013). Here we used an organic NO_2^+/NO^+ ratio that was equal to the ammonium nitrate NO_2^+/NO^+ ratio from our calibrations divided by 2.8. This factor was determined from multiple datasets (see discussion in Supplemental Information). The ammonium nitrate NO_2^+/NO^+ ratio was obtained from the two calibrations on 30 June and 7 July

that bracketed the flight on 2 July, which is analyzed here. It was 0.514 and 0.488, respectively, and for all of the data from both calibrations it averaged 0.490. Hence, the organic nitrate NO_2^+/NO^+ ratio was estimated to be 0.175. This is the first time, to our knowledge, that UMR measurements of aerosol nitrate have been corrected with HR correlations and used to apportion the corrected nitrate into inorganic or organic nitrate species.

The time since emission of intercepted power plant plumes was estimated from the slope of a plot of O_3 against NO_2. For nighttime emitted NO_x plumes that consist primarily of NO (Peischl et al., 2010), O_3 is negatively correlated with NO_2 due to the rapid reaction of NO with O_3 that produces NO_2 in a 1:1 ratio:

$$NO + O_3 \rightarrow NO_2 + O_2 \quad \text{(R1)}$$

Reaction R1 goes rapidly (NO pseudo first order loss rate coefficient of 0.03 s^{-1} at 60 ppb O_3) to completion, so that all NO_x is present as NO_2, as long as the plume NO does not exceed background O_3 after initial mixing of the plume into background air. Subsequent oxidation of NO_2 via reaction (R2) leads to an increasingly negative slope of O_3 vs NO_2:

$$NO_2 + O_3 \rightarrow NO_3 + O_2 \quad \text{(R2)}$$

Equation (1) then gives plume age subsequent to the completion of (R1) in terms of the observed slope, *m*, of O_3 vs NO_2 (Brown et al., 2006).

$$t_{plume} = \frac{ln[1-S(m+1)]}{Sk_1\overline{O_3}} \quad (1)$$

Here *S* is a stoichiometric factor that is chosen for this analysis to be 1 based on agreement of plume age with elapsed time in a box model run initialized with SENEX flight conditions (see below); k_1 is the temperature dependent bimolecular rate constant for $NO_2 + O_3$ (R2) and $\overline{O_3}$ is the average O_3 within the plume.

We calculate plume ages using both a stoichiometric factor of 1 (loss of NO_3 and N_2O_5 dominated by NO_3 reactions) and 2 (loss dominated by N_2O_5 reactions), although we note that the chemical regime for NO_3+N_2O_5 loss may change over the lifetime of the plume, progressing from 1 to 2 as the BVOC is consumed. We use *S*=1 values in the analysis that follows. Because the more aged plumes are more likely to have *S* approach 2, this means that some of the older plumes may have overestimated ages. Fig. S3 in the Supplemental Information shows the plume age calculated by Eq. 1 using modeled NO_x, NO_y and O_3 concentrations for *S*=1 and *S*=2, from nighttime simulations of plume evolution using an observationally constrained box model. This confirms that for nighttime plumes, *S*=1 plume ages match modeled elapsed time well. The model used for this calculation, and those used to assess peroxy radical lifetimes and fates in Section 4.3, was the Dynamically Simple Model of Atmospheric Chemical Complexity (DSMACC (Emmerson and Evans, 2009)) containing the Master Chemical Mechanism v3.3.1 chemistry scheme (Jenkin et al., 2015). More details on the model approach are provided in the SI.

3 Nighttime flight selection

There were three nighttime flights (takeoffs on the evenings of 19 June, 2 July, and 3 July, 2013, local time) conducted during SENEX, of which one (2 July) surveyed regions surrounding Birmingham, Alabama, including multiple urban and power plant plume transects. As described in the introduction, these plume transects are the focus of the current analysis since they correspond to injections of concentrated NO (and subsequently high $P(NO_3)$) into the regionally widespread residual layer isoprene. The nighttime flight on 3 July, over Missouri, Tennessee and Arkansas sampled air more heavily influenced by biomass burning than biogenic emissions. The 19 June night flight sampled earlier in the evening, in the few hours immediately after sunset, and sampled more diffuse urban plume transects that had less contrast with background air. Therefore, this paper uses data exclusively from the 2 July flight, in which 9 transects of well-defined NO_x plumes from power plants emitted during darkness can be analyzed to obtain independent yields measurements.

A map of the 2 July flight track is shown in Fig. 1a. After takeoff at 8:08 pm local Central Daylight Time on 2 July, 2013 (1:08 am UTC 3 July, 2016), the flight proceeded towards the southwest until due west of Montgomery, AL, after which it conducted a series of east-west running tracks while working successively north toward Birmingham, AL. Toward the east of Birmingham, the aircraft executed overlapping north-south tracks at six elevations to sample the E. C. Gaston power plant. During the course of the flight, concentrated NO_x plumes from the Gaston, Gorgas, Miller and Greene City power plants were sampled. Around 1:30 and 2:30 AM Central Daylight Time (5:30 and 6:30 am UTC), two transects of the Birmingham, AL urban plume were measured prior to returning to the Smyrna, TN airport base.

The flight track is shown colored by the nitrate radical production rate, $P(NO_3)$, to show the points of urban and/or power plant plume influence:

$$P(NO_3) = k_2(T)\,[NO_2][O_3] \quad (2)$$

Here, k_2 is again the temperature-dependent rate coefficient for reaction of $NO_2 + O_3$ (Atkinson et al., 2004), and the square brackets indicate concentrations. Fig. 1b further illustrates the selection of power plants plumes: sharp peaks in $P(NO_3)$ are indicative of power plant plume transects, during which isoprene mixing ratios also are observed to drop from the typical regional residual layer background values of ~ 1 ppb, indicative of loss by NO_3 oxidation (an individual transect is shown in more detail below in Fig. 2). Also shown in Fig. 1b are measured concentrations of isoprene and monoterpenes throughout the flight, showing substantial residual layer isoprene and supporting the assumption that effectively all NO_3 reactivity is via isoprene (see calculation in next section). Residual layer concentrations of other VOCs that could produce SOA (e.g., aromatics) are always below 100 pptv, and their reaction rates with NO_3 are slow. Edwards *et al*. (Edwards et al., 2017) have shown that NO_3 and isoprene mixing ratios for this and other SENEX night flights exhibit a strong and characteristic anticorrelation that is consistent with nighttime residual layer oxidation chemistry.

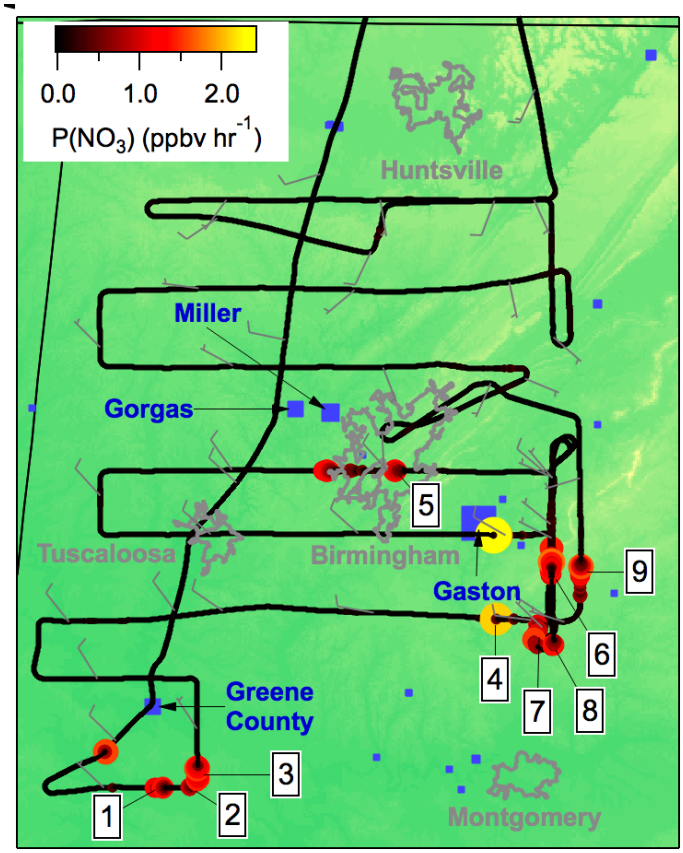

434 **1a**

435 **1b**

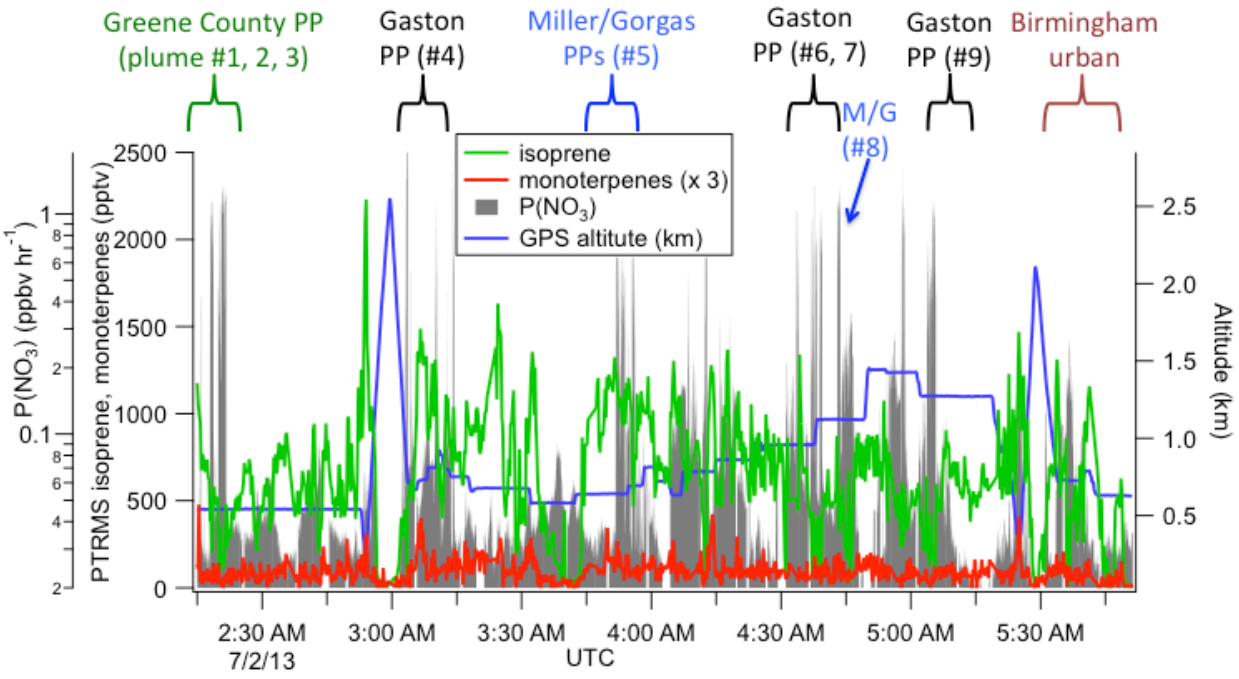

436

437 **Figure 1a.** Map of northern Alabama, showing the location of the flight track of the 2 July 2013
438 night flight used in the present analysis, with plume numbers labeled and wind direction shown.
439 Although the wind direction changed throughout the night, these measurements enable us to

attribute each plume to a power plant source (see labels in Figure 1b and Table 2). Color scale shows $P(NO_3)$ based on aircraft-measured $[NO_2]$ and $[O_3]$, while power plants discussed in the text are indicated in blue squares with marker size scaled to annual NO_x emissions for 2013 (scale not shown). Isoprene emissions are widespread in the region (Edwards et al., 2017). **Figure 1b** shows time series data from the same flight, with plume origins and numbers labeled, showing aircraft-measured isoprene and monoterpene concentrations, altitude, and $P(NO_3)$ determined according to Eq. 2 (log scale), showing that the isoprene was uniformly distributed (mixing ratios often in excess of 1 ppbv), while the more reactive monoterpenes were present at mixing ratios below 100 ppt except at the lowest few hundred meters above ground in the vertical profiles (not used in the present analysis). Figure 1b also shows that sharp peaks in nitrate radical production rate occur both at the lowest points of these vertical profiles, when the aircraft approached the surface, but also frequently during periods of level flight in the residual layer, which correspond to the power plant plume transects analyzed in this paper.

4 Results

4.1 Selection of plumes

Figure 2 shows a subset of the July 2 flight time series data, illustrating three NO_x plumes used for analysis. The large NO_3 source and isoprene loss was accompanied by an increase in organic nitrate aerosol mass, which we attribute to the NO_3 + isoprene reaction based on prior arguments. We observed each plume as a rapid and brief perturbation to background conditions, of order 10 – 50 sec., or 1 – 5 km in spatial scale. Each plume's perturbed conditions can correspond to different plume ages, depending on how far downwind of the power plant the plume transect occurred.

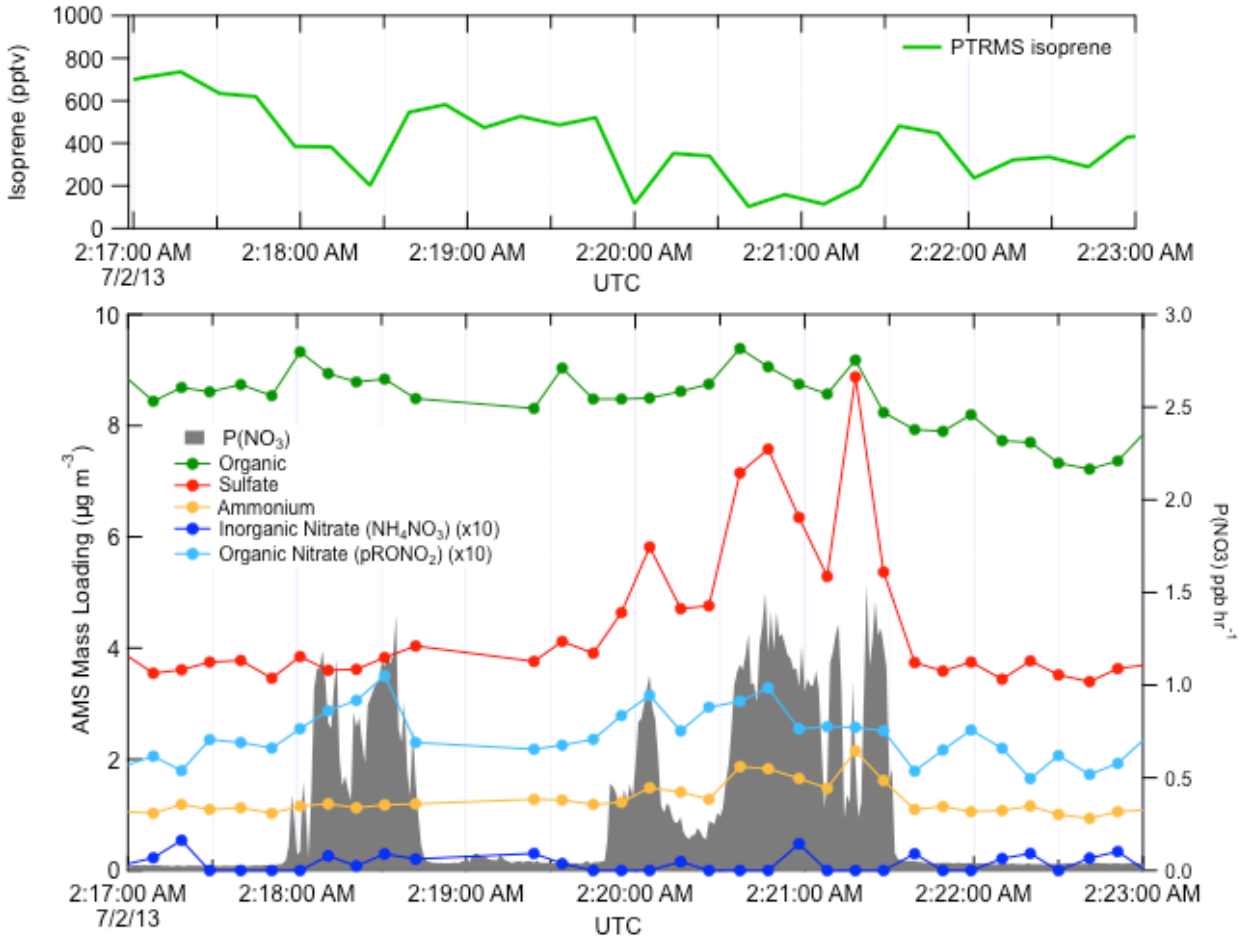

Figure 2. Three representative plume transect observations from the 2 July 2013 flight (plumes are identified by the peaks in $P(NO_3)$, listed in Table 1 at times 02:18, 02:20, and 02:21 UTC). Note the difference in sulfate enhancement in the three plumes, which is largest in the third plume, and is accompanied by increases in ammonium. In all three cases, the isoprene concentration drops in the plumes, accompanied by a clear increase in organic nitrate, no changes in the inorganic nitrate, and a modest changes in organic aerosol mass concentrations.

Candidate plumes were initially identified by scanning the time series flight data for any period where the production rate of nitrate radical ($P(NO_3)$) rose above 0.5 ppbv hr^{-1}. This threshold was chosen to be above background noise and large enough to isolate only true plumes (see Fig. 1a). The value is thus subjectively chosen, but was consistently applied across the dataset. For each such period, a first screening removed any of these candidate plumes that occurred during missed approaches or other periods where radar altitude above ground level (AGL) was changing, because in the stratified nighttime boundary layer structure, variations in altitude may result in sampling different air-masses, rendering the adjacent out of plume background not necessarily comparable to in-plume conditions. A second criterion for rejection of a plume was missing isoprene or AMS data during brief plume intercepts. No selected plumes on July 2 showed enhanced acetonitrile or refractory black carbon, indicating no significant biomass

burning influence. Finally, two plumes downwind of the Gaston power plant (at 03:10 and 03:14) were removed from the present analysis, because (03:10) the background isoprene was changing rapidly, preventing a good baseline measurement, and (03:14) there was no observed decrease in isoprene concentration in-plume (as well as no increase in nitrate aerosol). The 03:14 plume was apparently too recently emitted to have undergone significant nighttime reaction; its O_3/NO_2 slope was unity to within the combined measurement error of O_3 and NO_2 (Eq. 1). After this filtering, there are 9 individual plume observations for determination of NO_3 + isoprene SOA yields (see Table 1). The rapid increases in $P(NO_3)$ appeared simultaneously with significant decreases in isoprene and increases in aerosol nitrate. The aerosol and isoprene measurements (taken at data acquisition rates < 1 Hz) were not exactly coincident in time which leads to some uncertainty in the yield analysis below.

Derivation of SOA yields from observed changes in isoprene and aerosol mass in plumes depends on two conditions, and has several caveats that will be discussed in the text that follows (see Table 3 below for a summary of these caveats). The two conditions are: (1) that the majority of VOC mass consumed by NO_3 in plumes is isoprene (rather than monoterpenes or other VOC), and then either or both (2a) that the change in aerosol organic mass concentration during these plumes is due to NO_3 + isoprene reactions, and/or (2b) that the change in aerosol nitrate mass concentration is due to NO_3 + isoprene reactions. There are separate considerations for each of these conditions.

For the first condition, we note that the isoprene to monoterpenes ratio just outside each plume transect was always high (a factor of 10 to 70, on average 26). With the 298 K NO_3 rate constants of ~ 5×10^{-12} cm^3 $molec^{-1}$ s^{-1} for monoterpenes and 6.5×10^{-13} cm^3 $molec^{-1}$ s^{-1} for isoprene (Calvert et al., 2000), isoprene (~ 2 ppb) will always react faster with nitrate than monoterpenes (~ 0.04 ppbv). At these relative concentrations, even if all of the monoterpene is oxidized, the production rate of oxidation products will be much larger for isoprene. Contribution to aerosol by N_2O_5 uptake is also not important in these plumes. Edwards et al. (Edwards et al., 2017) calculated the sum of NO_3 and N_2O_5 loss throughout this flight and showed that it is consistently NO_3+BVOC dominated (Fig. S4 of that paper). As isoprene depletes, N_2O_5 uptake will increasingly contribute to NO_3 loss, but as shown below, we are able to rule out a substantial source of inorganic nitrate for most plumes. We also know that despite increased OH production in-plume, the isoprene loss is still overwhelming dominated by NO_3 (Fig. S5 in Edwards, et al. (Edwards et al., 2017)) .

The second condition requires that we can find an aerosol signal that is attributable exclusively to NO_3 + isoprene reaction products, whether it be organic aerosol (OA) or organic nitrate aerosol ($pRONO_2$) mass loading, or both. We note that the ratio of in-plume aerosol organic mass increase to $pRONO_2$ mass increase is noisy (see discussion below at Fig. 6), but indicates an average in-plume ΔOA to $\Delta pRONO_2$ ratio of about 5. The large variability is primarily due to the fact that the variability in organic aerosol mass between successive 10-second data points for the entire flight is quite large (of order 0.75 μg m^{-3}) and comparable to many of the individual plume ΔOA increases, far exceeding the expected organonitrate driven increases in OA, which are roughly twice the $pRONO_2$ mass increases. It is also possible that in these plumes, where

total aerosol mass is elevated, semivolatile organic compounds may re-partition to the aerosol phase, contributing a non-$pRONO_2$ driven variability in ΔOA. For example, if some gas phase IEPOX is present in the residual layer, it may be taken up into the highly acidic aerosol from the power plants. Alternatively, very polar gas-phase compounds could partition further into the higher liquid water associated with the sulfate in the plume. Therefore, in-plume organic aerosol increases cannot be attributed clearly to NO_3 + isoprene SOA production, so we do not use them in the SOA yield calculations.

This leaves consideration 2b, whether all increase in nitrate mass is due to NO_3 + isoprene reactions. Here we must evaluate the possibility of inorganic nitrate aerosol production in these high-NO_x plumes. Fine-mode aerosol inorganic nitrate can be formed by the (reversible) dissolution of $HNO_{3(g)}$ into aqueous aerosol. In dry aerosol samples, inorganic nitrate is typically in the form of ammonium nitrate (NH_4NO_3), when excess ammonium is available after neutralization of sulfate as $(NH_4)_2SO_4$ and $NH_4(HSO_4)$. Because of the greater stability of ammonium sulfate salt relative to ammonium nitrate, in high-sulfate plumes with limited ammonium, inorganic nitrate aerosol will typically evaporate as $HNO_{3(g)}$ (Guo et al., 2015) (reaction R3):

$$2NH_4NO_{3(aq)} + H_2SO_{4(aq)} \rightleftarrows (NH_4)_2SO_{4(aq)} + 2HNO_{3(g)} \quad \text{(R3)}$$

Inorganic nitrate can also form when crustal dust (e.g. $CaCO_3$) or seasalt (NaCl) are available. Uptake of HNO_3 is rendered favorable by the higher stability of nitrate mineral salts, evaporating CO_2 or HCl. Inorganic nitrate can also be produced by the heterogeneous uptake of N_2O_5 onto aqueous aerosol; Edwards et al. (2017) demonstrated that this process is negligible relative to NO_3 + BVOC for the July 2 SENEX night flight considered here.

There are several lines of evidence that the observed nitrate aerosol is organic and not inorganic. First, examination of the NO_2^+/NO^+ (interference-corrected *m/z* 46:*m/z* 30) ratio measured by the aircraft AMS (Fig. 3) shows a ratio throughout the July 2 flight, including the selected plumes, that is substantially lower than that from the bracketing ammonium nitrate calibrations. This lower AMS measured NO_2^+/NO^+ ratio has been observed for organic nitrates (Farmer et al., 2010), and some mineral nitrates (e.g. $Ca(NO_3)_2$ and $NaNO_3$, (Hayes et al., 2013)), which are not important in this case because aerosol was dominantly submicron. As described above, we can separate the observed AMS nitrate signal into $pRONO_2$ and inorganic nitrate contributions. These mass loadings are also shown in Fig. 3, indicating dominance of $pRONO_2$ throughout the flight.

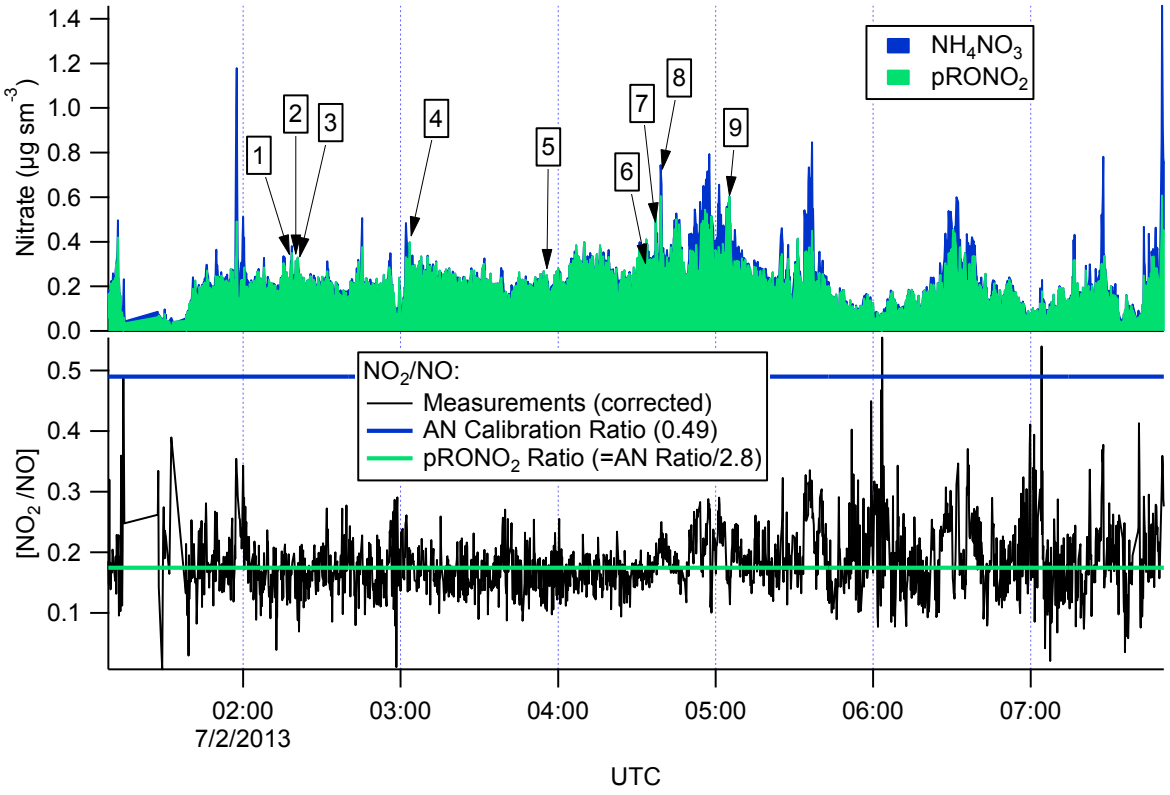

Figure 3. For the flight under consideration, the estimated relative contributions of ammonium and organic nitrate to the total corrected nitrate signal (top panel) was calculated from the ratios of the corrected peaks at *m/z* 30 and 46 (lower panel). Each of the plumes is identified here by plume number. The ratios of NO_2^+/NO^+ (black data in the lower panel) from the corrected peaks at *m/z* 46 and 30, respectively, are compared to the ratios expected for ammonium nitrate (AN Calibration Ratio, blue horizontal line at 0.49) or organic nitrate ($pRONO_2$ Ratio, green horizontal line at 0.175 which is estimated from the AN calibration ratio using multiple data sets (see discussion in Supplemental Information). The measured ratio for most of the flight is more characteristic of organic nitrate than ammonium nitrate.

We can also employ the comparison of other AMS-measured aerosol components during the individual plumes to assess the possibility of an inorganic nitrate contribution to total measured nitrate. Fig. S5a shows that the in-plume increases in sulfate are correlated with increases in ammonium with an R^2 of 0.4. The observed slope of 5.4 is characteristic of primarily $(NH_4)HSO_4$, which indicates that the sulfate mass is not fully neutralized by ammonium. We note, however, that if the largest observed aerosol nitrate increase is due solely to ammonium nitrate, the ammonium increase would be only 0.11 µg m^{-3}, which would be difficult to discern from the NH_4 variability of order 0.11 µg m^{-3}. However, the slope is consistent with incomplete neutralization of the sulfate by ammonium, which would make $HNO_{3(g)}$ the more thermodynamically favorable form of inorganic nitrate. The ion balance for the ammonium nitrate calibration particles and the plume enhancements are shown in Fig. S5b. Complete neutralization of the calibration aerosols is nearly always within the gray 10% uncertainty band for the relative ionization efficiency of

ammonium (Bahreini et al., 2009). In contrast, many of the plume enhancements are near the 1:2 line (as primarily ammonium bisulfate) within the combined 10% ammonium and 15% sulfate uncertainty error bars or without ammonium (sulfuric acid). Thus, NH_4NO_3 is unlikely to be stable in the aerosol phase under the conditions of these plumes, consistent with the AMS observations.

A plot of the calculated plume enhancements from the derived apportionment into organic ($pRONO_2$) and inorganic (ammonium) nitrate is shown in Fig. 4. The increases in aerosol nitrate for nearly all of the plumes appear to be mostly due to enhancements in pRONO2. Based on these considerations, we conclude that in-plume $pRONO_2$ mass increases are a consequence (and thus a robust measure) of organic nitrate aerosol produced from NO_3 + isoprene. Since each isoprene molecule condensing will have one nitrate group, the ratio of these increases to isoprene loss is a direct measure of the molar organic aerosol yield from NO_3-isoprene oxidation.

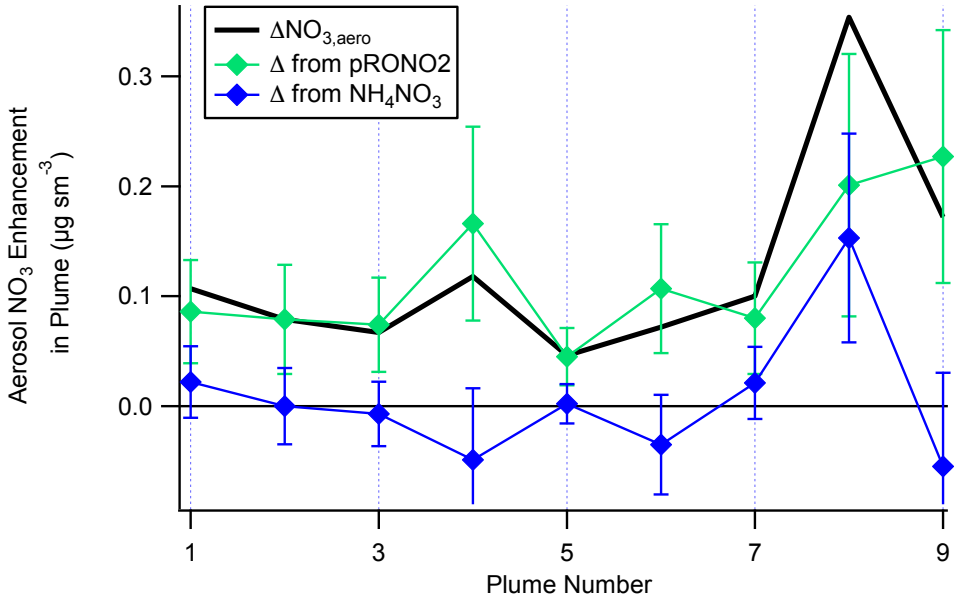

Figure 4. The contribution of each species to the nitrate enhancements in each of the plumes, showing that the enhancements in most of the plumes are mainly due to enhancements in organic nitrate, with the exception of Plume 8 which had enhancements in both organic and ammonium nitrate. Error bars are estimated from the measurement variability, the UMR corrections to the nitrate signals, apportionment between organic and inorganic nitrate, and the total nitrate uncertainty (see Supplemental Information).

Table 1 shows the selected plumes to be used for yield analysis. Wherever possible, multiple points have been averaged for in-plume and background isoprene and nitrate aerosol concentrations; in each case the number of points used is indicated and the corresponding standard deviations are reported. In two cases (2:20 and 3:03 plumes), the plumes were so narrow that only a single point was measured in-plume at the 10 s time resolution of the PTR-

MS and AMS; for these “single-point” plumes it is not possible to calculate error bars. Error bars were determined using the standard deviations calculated for in-plume and background isoprene and nitrate aerosol concentrations, accounting also for the additional uncertainty in the AMS measurement described in the caption to Figure 4, and propagated through the yield formula detailed in the following section.

Table 1. List of plumes used in this NO_3 + isoprene SOA yield analysis. For each plume, the delta-values listed indicate the difference between in-plume and outside-plume background in average observed concentration, and the standard deviations (SD) are the propagated error from this subtraction. (For ΔNO_3 from $pRONO_2$, the standard deviations also include error propagated as described in the caption for Figure 4) After each plume number, the numbers of points averaged for isoprene (10 s resolution) and AMS (10 s resolution), respectively, are listed. Because the isoprene data were reported at a lower frequency, these numbers are typically lower to cover the same period of time. Plume numbers annotated with * indicate brief plumes for which only single-point measurements of in-plume aerosol composition were possible. Additional AMS and auxiliary data from each plume is included in the Supplemental Information, Table S3.

plume number [#isop/#AMS]	**7/2/13 plume time (UTC)**	**$P(NO_3)$ (ppbv hr^{-1})**	**ΔISOP (ppt) [± SD]**	**$\Delta NO_{3,aero}$ (μg m^{-3}) [± SD]**	**ΔNO_3 from $pRONO_2$ (μg m^{-3}) [± SD]**	**ΔNO_3 from NH_4NO_3 (μg m^{-3}) [± SD]**
Typical variability (μg m^{-3}):				0.05	0.05	0.05
1 [2/3]	2:18	0.9	-335 [128]	0.107 [0.039]	0.086 [0.047]	0.022 [0.012]
2 [*]	2:20	0.8	-404	0.079	0.079 [0.049]	0
3 [4/5]	2:21	1.2	-228 [121]	0.067 [0.039]	0.074 [0.043]	-0.007 [0.027]
4 [*]	3:03	1.4	-453	0.118	0.166 [0.088]	-0.049
5** [3/4]	3:55	1.0	-255 [251]	0.046 [0.019]	0.045 [0.026]	0.002 [0.015]
6 [2/2]	4:34	0.6	-713 [219]	0.072 [0.031]	0.107 [0.059]	-0.035 [0.029]
7 [5/6]	4:37	0.8	-298 [197]	0.100 [0.082]	0.080 [0.051]	0.021 [0.034]
8*** [2/3]	4:39	0.9	-443 [75]	0.354 [0.058]	0.201 [0.120]	0.153 [0.057]
9 [7/8]	5:04	0.6	-293 [131]	0.172 [0.048]	0.227 [0.115]	-0.055 [0.042]

**Plume 5 has the smallest $\Delta NO_{3,aero}$ and may be affected by background $pRONO_2$ variability.
***Plume 8 has a measurable increase in inorganic nitrate as well as organic.

4.2 SOA yield analysis

A **molar** SOA yield refers to the number of molecules of aerosol organic nitrate produced per molecule of isoprene consumed. In order to determine molar SOA yields from the data presented in Table 1, we convert the aerosol organic nitrate mass loading differences to mixing ratio differences (ppt) using the NO_3 molecular weight of 62 g mol^{-1} (the AMS organic nitrate

mass is the mass only of the $-ONO_2$ portion of the organonitrate aerosol). At standard conditions of 273 K and 1 atm (all aerosol data are reported with this STP definition), 1000 ppt NO_3 = 2.77 μg m^{-3}, so each ΔM_{pRONO2} is multiplied by 361 ppt (μg m^{-3})$^{-1}$ to determine this molar yield:

$$Y_{SOA,molar} = \frac{(pRONO2_{plume} \pm SD_{pRONO2plume}) - (pRONO2_{bkg} \pm SD_{pRONO2bkg})}{-[(isop_{plume} \pm SD_{isopplume}) - (isop_{bkg} \pm SD_{isopbkg})]} \times \frac{361\ ppt\ NO_3}{\mu g\ m^{-3}} \quad (3)$$

The SOA molar yields resulting from this calculation are shown in Table 2, spanning a range of 5-28%, with uncertainties indicated based on the SDs in measured AMS and isoprene concentrations. In addition to this uncertainty based on measurement precision and ambient variability, there is an uncertainty of 50% in the AMS derived-organic nitrate mass loadings (see SI) and 25% in the PTR-MS isoprene concentrations (Warneke et al., 2016). The average molar $pRONO_2$ yield across all plumes, with each point weighed by the inverse of its standard deviation, is 9%. (As noted below, the yield appears to increase with plume age, so this average obscures that trend.) An alternate graphical analysis of molar SOA yield from all nine plumes plus one 'null' plume (03:14, in which no isoprene had yet reacted and thus not included in Tables 1 and 2) obtains the same average molar yield of 9% (Fig. 5). Here, the molar yield is the slope of a plot of plume change in $pRONO_2$ vs plume change in isoprene. The slope is determined by a linear fit with points weighted by the square root of the number of AMS data points used to determine in-plume $pRONO_2$ in each case. This slope error gives a rather narrow uncertainty range for the slope (0.0930 +/- 0.0011); to obtain an upper limit in the uncertainty of this molar yield we apply the combined instrumental uncertainties, based on adding in quadrature the PTR-MS uncertainty of 5% and the AMS uncertainty of 50%. This gives an overall uncertainty of 50.2%, resulting in upper and lower limit slopes of 0.140 and 0.046, respectively; we use this maximum uncertainty estimate to report the average molar yield as 9% (+/- 5%). We have not corrected the calculated yields for the possibility of NO_3 heterogeneous uptake, which could add a nitrate functionality to existing aerosol. Such a process could be rapid if the uptake coefficient for NO_3 were 0.1, a value characteristics of unsaturated substrates (Ng et al., 2017), but would not contribute measurably at more conventional NO_3 uptake coefficients of 0.001 (Brown and Stutz, 2012).

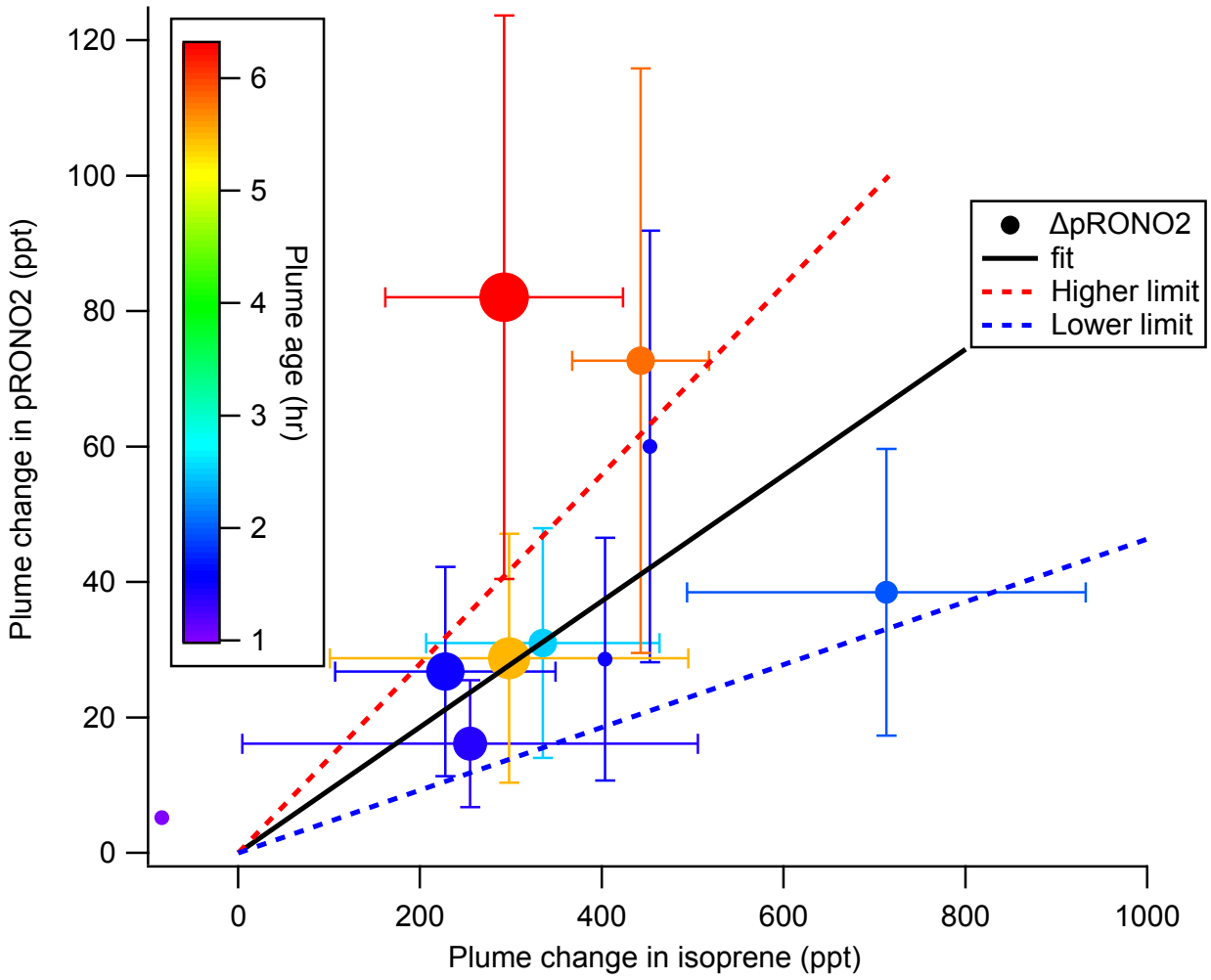

Figure 5. SOA molar yield can be determined as the slope of $\Delta pRONO_2$ vs. Δisoprene, both in mixing ratio units. The linear fit is weighted by square root of number of points used to determine each in-plume $pRONO_2$, with intercept held at zero. The slope coefficient ± one standard deviation is 0.0930 ± 0.0011. Larger "outside" high and low limits of the slope (shown as dashed red and blue lines) are obtained by adding and subtracting from this slope the combined instrumental uncertainties, based on adding in quadrature the PTR-MS uncertainty of 5% and the AMS uncertainty of 50%. This gives an overall uncertainty of 50.2%, resulting in upper and lower limit slopes of 0.140 and 0.046, respectively. Points are colored by plume age, and size scaled by square root of number of points (the point weight used in linear fit). This plot and fit includes the nine plumes listed in Tables 1 and 2, as well as the 03:14 "unreacted" plume (at Δisoprene = -84 ppt). Error bars on isoprene are the propagated standard deviations of the (in plume - out plume) differences, for plumes in which multi-point averages were possible. Error bars on pRONO2 are the same as in Figure 4, converted to ppt. The points without error bars are single-point plumes.

To estimate SOA **mass** yields, we need to make some assumption about the mass of the organic molecules containing the nitrate groups that lead to the observed nitrate aerosol mass increase. The observed changes in organic aerosol are too variable to be simply interpreted as the organic portion of the aerosol organic nitrate molecules. We conservatively assume the organic mass to be approximately double the nitrate mass (62 g mol^{-1}), based on an "average" molecular structure of an isoprene nitrate with 3 additional oxygens: e.g. a tri-hydroxynitrate (with organic portion of formula $C_5H_{11}O_3$, 119 g mol^{-1}), consistent with 2nd-generation oxidation product structures suggested in Schwantes, et al. (Schwantes et al., 2015). Based on this assumed organic to nitrate ratio, all plumes' expected organic mass increases would be less than the typical variability in organic of 0.75 μg m^{-3}. This assumed structure is consistent with oxidation of both double bonds, which appears to be necessary for substantial condensation of isoprene products, and which structures would have calculated vapor pressures sufficiently low to partition to the aerosol phase (Rollins et al., 2009). Another possible route to low vapor pressure products is intramolecular H rearragement reactions, discussed below in Section 4.3, which would not require oxidant reactions at both double bonds. In the case of oxidant reactions at both double bonds, it is difficult to understand how the second double bond would be oxidized unless by another nitrate radical, which would halve these assumed organic to nitrate ratios (assuming the nitrate is retained in the molecules). On the other hand, any organic nitrate aerosol may lose NO_3 moieties, increasing the organic to nitrate ratio. Given these uncertainties in both directions, we use the assumed "average" structure above to guess an associated organic mass of double the nitrate mass. Thus, to estimate SOA mass yield, we multiply the increase in organic nitrate aerosol mass concentration by three (i.e., $2 \times \Delta M_{pRONO2} + \Delta M_{pRONO2}$), and divide by the observed decrease in isoprene, converted to μg m^{-3} by multiplying by 329 ppt (μg m^{-3})$^{-1}$, the conversion factor based on isoprene's molecular weight of 68.12 g mol^{-1}.

$$Y_{SOA,mass} = \frac{(pRONO2_{plume} \pm SD_{pRONO2plume}) - (pRONO2_{bkg} \pm SD_{pRONO2bkg})}{-[(isop_{plume} \pm SD_{isopplume}) - (isop_{bkg} \pm SD_{isopbkg})]} \times 3 \times \frac{329ppt}{\mu g\ m^{-3}} \quad (4)$$

Note that the SOA mass yield reported here is based on the (assumed) mass of organic aerosol plus the (organo)nitrate aerosol formed in each plume. If instead the yield were calculated using only the assumed increase in ***organic*** mass (i.e., 2x ΔM_{pRONO2} instead of 3x ΔM_{pRONO2}), which would be consistent with the method used in Rollins, et al. (Rollins et al., 2009) and Brown et al. (Brown et al., 2009), the mass yields would be 2/3 the values reported here. However, since SOA mass yield is typically defined based on the total increase in aerosol mass, we use the definition with the sum of the organic and nitrate mass here. This results in an average SOA mass yield of 27%, with propagated instrumental errors (see caption to Fig. 5) giving a range of 27% +/- 14%.

We note also that correlation of in-plume increases in OA with $pRONO_2$ (Fig. 6) point to a substantially larger 5:1 organic-to-nitrate ratio; if this were interpreted as indicating that the average molecular formula of the condensing organic nitrate has 5 times the organic mass as nitrate, this would increase the SOA mass yields reported here. However, due to the aforementioned possibility of additional sources of co-condensing organic aerosol, which led us to avoid using ΔOA in determining SOA yields, we do not consider this to be a direct indication

of the molecular formula of the condensing organic nitrate. Including OA in the SOA yield determination, based on this 5:1 slope rather than the assumed 2:1 OA:$pRONO_2$, would give 2.5 times larger SOA mass yields than reported here.

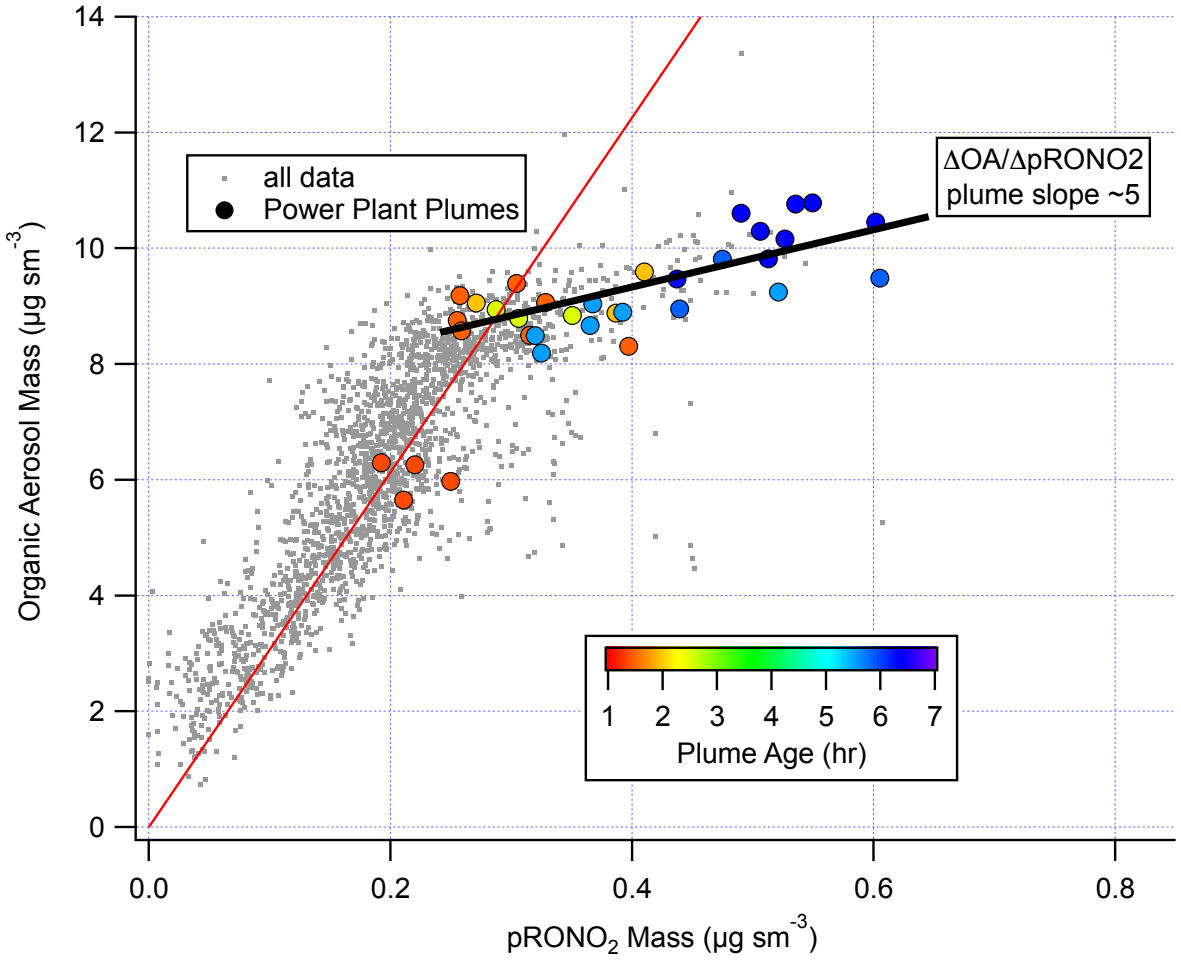

Figure 6. Correlation of organic aerosol mass concentration with $pRONO_2$ mass concentration for the full 2 July flight (grey points and red fit line, fitted slope and thus average OA/$pRONO_2$ mass ratio of ~30) and for the points during the selected plumes (colored points, colored by plume age, average OA/$pRONO_2$ mass ratio of ~ 5).

Table 2. SOA Yields for each plume observation, estimated plume age, and likely origin. See text for description of uncertainty estimates. For the mass yields, the calculated SOA mass increase includes both the organic and (organo)nitrate aerosol mass; the measurements for OA increases shown in Figure 6 do not include the nitrate mass.

plume number	plume time (UTC)	SOA molar yield (fraction) [± SD]	SOA mass yield (fraction) [± SD]	plume age from O_3/ NO_2 clock assuming S=1 (hours)	Likely NOx origin & altitude (m)
1	7/2/13 2:18	0.09 [0.06]	0.25 [0.17]	2.5	Greene County @ 540 m
2	7/2/13 2:20	0.07	0.21	1.5	*ibid*
3	7/2/13 2:21	0.12 [0.10]	0.32 [0.25]	1.5	*ibid*
4	7/2/13 3:03	0.13	0.36	1.5	Gaston @ 720 m
5	7/2/13 3:55	0.06 [0.07]	0.17 [0.20]	1.4	Miller / Gorgas @ 690 m
6	7/2/13 4:34	0.05 [0.03]	0.15 [0.09]	2	*ibid*
7	7/2/13 4:37	0.10 [0.09]	0.26 [0.24]	5.5	*ibid*
8	7/2/13 4:39	0.16 [0.10]	0.45 [0.28]	5.8	Miller / Gorgas @ 1120 m
9	7/2/13 5:04	0.28 [0.19]	0.77 [0.52]	6.3	Gaston @ 1280 m

748 **Table 3.** Several caveats to the present SOA yields analysis are listed below, alongside the
749 expected direction each would adjust the estimated yields. Because we do not know whether or
750 how much each process may have occurred in the studied plumes, we cannot quantitatively
751 assess the resulting uncertainties, so we simply list them here. See text above for more detailed
752 discussion.

Process	Effect on determined SOA yield
Organic nitrate aerosol loses NO_3 functional group	Larger, because the non-nitrate OA would not be counted in this analysis
Both double bonds in isoprene are oxidized by NO_3: two nitrates per condensing molecule	Smaller, because the assumed organic to nitrate mass ratio assumes one nitrate per molecule
NO_3 oxidizes daytime isoprene oxidation products (e.g. ISOPOOH) to make new aerosol	Smaller, because this would produce organic nitrate aerosol without corresponding decrease in isoprene, so that some of existing SOA production is mis-attributed to isoprene + NO_3
Assumed organic to nitrate mass ratio is incorrect	Unknown direction of effect, depends on whether assumed ratio is high or low
Daytime-produced IEPOX uptake onto acidic particles	No effect (only changes ΔOA, not nitrate)
Suppression of O_3 + monoterpene or O_3 + isoprene SOA in plumes	No effect (only changes ΔOA, not nitrate)

753
754 Finally, the large range in observed yields can be interpreted by examining the relationship to
755 estimated plume age. Using the slope of O_3 to NO_2 (Eq. 1) to estimate plume age as described
756 above, a weak positive correlation is observed (Table 2, Fig. S4), suggesting that as the plume
757 ages, later-generation chemistry results in greater partitioning to the condensed phase of NO_3 +
758 isoprene organonitrate aerosol products. This is consistent with the observation by Rollins et al.
759 (Rollins et al., 2009) that 2nd-generation oxidation produced substantially higher SOA yields
760 than the oxidation of the first double bond alone, but we note that these mass yields (averaging
761 27%, would be 18% using the organic mass only) are higher than even the largest yield found in
762 that chamber study (14%, used organic mass only).
763
764 We observe increasing SOA yield, from a molar yield of around 10% at 1.5 hours up to 30% at 6
765 hours of aging. The lowest yields observed are found in the most recently emitted plumes,
766 suggesting the interpretation of the higher yields as a consequence of longer aging timescales
767 in the atmosphere.

768 4.3 Mechanistic considerations

769
770 These larger SOA mass yields from field determinations (average 27%) relative to chamber
771 work (12 – 14%, see introduction) may arise for several reasons. We first assess the volatility of
772 assumed first- and second-generation products using group contribution theory in order to
773 predict partitioning. After a single oxidation step, with a representative product assumed to be a

C_5 hydroperoxynitrate, the saturation vapor pressure estimated by group contribution theory (Pankow and Asher, 2008) at 283 K would be 2.10 x 10^{-3} Torr (C* = 1.7 x 10^4 μg m^{-3} for MW = 147 g mol^{-1}), while a double-oxidized isoprene molecule (assuming a C_5 dihydroxy dinitrate) has an estimated vapor pressure of 7.95 x 10^{-8} Torr (C* = 1.01 μg m^{-3} for MW = 226 g mol^{-1}). This supports the conclusion that while the first oxidation step produces compounds too volatile to contribute appreciably to aerosol formation, oxidizing both double bonds of the isoprene molecule is sufficient to produce substantial partitioning, consistent with Rollins et al. (Rollins et al., 2009). This is also true if the second double bond is not oxidized by nitrate (group contribution estimate P_{vap} for a C_5 tri-hydroxy nitrate is 7.7 x 10^{-8} Torr, C* = 0.79 μg m^{-3} for MW = 181 g mol^{-1}). These C* saturation concentration values suggest that no dimer formation or oligomerization is *required* to produce low-enough volatility products to condense to the aerosol phase; however, such oligomerization would result in more efficient condensation. The fact that Rollins et al. (Rollins et al., 2009) did not observe larger mass yields may indicate that it takes longer than a typical chamber experiment timescale to reach equilibrium, or that this absorptive partitioning model did not accurately capture those experiments, or that substantial loss of semivolatiles to the chamber walls (e.g. (Krechmer et al., 2016)) suppressed apparent yields.

Determination of yields from ambient atmospheric data differs from chamber determinations in several additional respects. First, ambient measurements do not suffer from wall loss effects, such that no corrections are necessary for loss of aerosol or semi-volatile gases (Matsunaga and Ziemann, 2010;Krechmer et al., 2016). Second, ambient measurements take place on the aging time scale of the atmosphere rather than a time scale imposed by the characteristics of the chamber or the choice of oxidant addition. Third, the typical lifetime of the initially produced nitrooxy-isoprene-RO_2 radical is more representative of the ambient atmosphere rather than a chamber. The unique conditions of a high NO_x power plant plume affect lifetime and fates of peroxy radicals, as described below.

To help interpret these in-plume peroxy radical lifetimes, a box model calculation using the MCM v3.3.1 chemistry scheme was run (see details in Supplemental Information). This box model shows substantially longer peroxy radical lifetimes during nighttime than daytime, initializing with identical plume-observed conditions. These long peroxy radical lifetimes may have consequences for comparison to chamber experiments: for example, in Schwantes' (Schwantes et al., 2015) chamber experiment on the NO_3 + isoprene reaction mechanism, the HO_2-limited nitrooxy-RO_2 lifetime was at maximum 30 s. In the plumes investigated in this study, peroxy radical lifetimes are predicted to be substantially longer (>200 s early in the night, see Fig. 7), allowing for the possibility of different bimolecular fates, or of unimolecular transformations of the peroxy radicals that may result in lower-volatility products (e.g., auto-oxidation to form highly oxidized molecules (Ehn et al., 2014)).

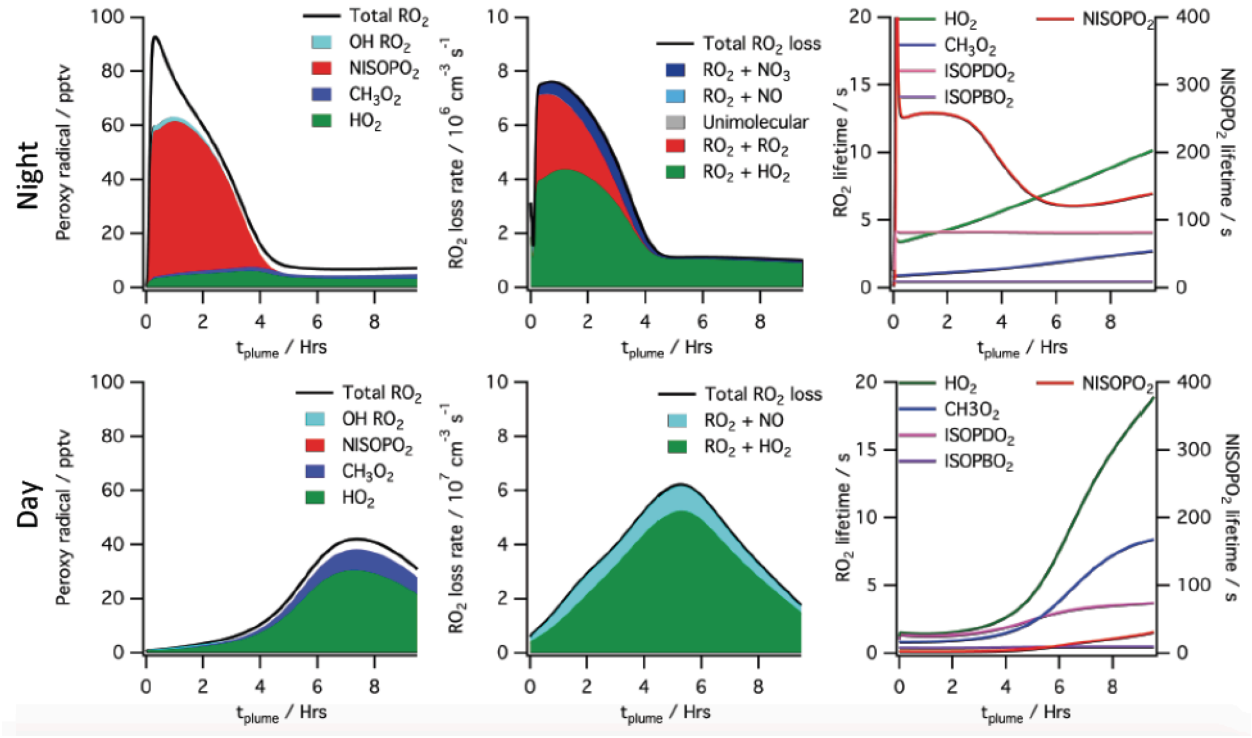

Figure 7. Simulated peroxy radical concentration (left), loss rates (middle), and lifetime (right), using the MCM v3.3.1 chemical mechanism, for conditions typical of a nighttime intercepted power plant plume (top) and the same plume initial conditions run for daytime simulation (bottom, local noon occurs at 5 hrs). Included are total peroxy radical concentration and losses, as well as the highlighted subclasses HO_2, CH_3O_2, total nitrooxy-isoprene-RO_2, and the total hydroxy-isoprene-RO_2 produced from OH oxidation. The righthand panels show HO_2, CH_3O_2 and the dominant hydroxy-isoprene-RO_2 $ISOPBO_2$ and $ISOPDO_2$ (β-hydroxy-peroxy radicals from OH attack at carbons 1 and 4 respectively) lifetime on the left axis and nitrooxy-isoprene-RO_2 on the right axis, showing nighttime lifetimes an order of magnitude longer than daytime for this NO_3 + isoprene derived RO_2 radical ($NISOPO_2$).

The typically assumed major fate of nighttime RO_2 in the atmosphere is reaction with HO_2 to yield a hydroperoxide, NO_3-ROOH. This is shown in the model output above as the green reaction, and is responsible for half of early RO_2 losses in the MCM modeled plume. Schwantes *et al*. (Schwantes et al., 2015) proposed reaction of these nighttime derived hydroperoxides with OH during the following day as a route to epoxides, which in turn can form SOA via reaction with acidic aerosol. Reaction of hydroperoxides with nighttime generated OH may similarly provide a route to SOA through epoxides, albeit more slowly than that due to photochemically generated OH.

The predicted longer nighttime peroxy radical lifetimes may enable unique chemistry. For example, if nitrooxy-isoprene-RO_2 self-reactions are substantially faster than assumed in the MCM, as suggested by Schwantes *et al*. (Schwantes et al., 2015), RO_2+RO_2 reactions may compete with the HO_2 reaction even more than shown in Fig. 7, and dimer formation may be favored at night, yielding lower volatility products. The 5:1 AMS Organic:Nitrate ratio observed in

the SOA formed in Rollins et al. (Rollins et al., 2009) , and consistent with aggregated observations reported here, may suggest that in some isoprene units the nitrate is re-released as NO_2 in such oligomerization reactions. We note that this larger organic to nitrate ratio would mean higher SOA mass yields than estimated in Table 2.

Alternatively, longer nighttime peroxy radical lifetimes may allow sufficient time for intramolecular reactions to produce condensable products. This unimolecular isomerization (auto-oxidation) of initially formed peroxy radicals is a potentially efficient route to low-volatility, highly functionalized products that could result in high aerosol yields. For OH-initiated oxidation of isoprene, laboratory relative rate experiments found the fastest 1,6-H-shift isomerization reaction to occur for the hydroxy-isoprene-RO_2 radical at a rate of 0.002 s^{-1} (Crounse et al., 2011), meaning that peroxy radicals must have an ambient lifetime of >500 s for this process to be dominant. As shown in Fig. 7, the simulated power plant plume peroxy radical lifetimes are long (>200 s), so an isomerization reaction at this rate may play a significant role. However, a recent study has demonstrated that OH-initiated and NO_3-initiated RO_2 radicals from the same precursor VOC can have very different unimolecular reactive fates due to highly structurally sensitive varying rates of reactions of different product channels (Kurtén et al., 2017). A similar theoretical study on the rate of unimolecular autooxidation reactions of nitrooxy-isoprene-RO_2 radicals would be valuable to help determine under what conditions such reactions might occur, and this knowledge could be applied to comparing chamber and field SOA yields.

4.4 Atmospheric implications and needs for future work

Because this paper proposes higher SOA yield for the NO_3 + isoprene reaction than measured in chamber studies, we conclude with some discussion of the implications for regional aerosol burdens, and further needs for investigation in the NO_3 + isoprene system.

Using an isoprene + NO_3 yield parameterization that gave a 12% SOA mass yield at 10 μg m^{-3}, Pye et al. (2010) found that adding the NO_3 + isoprene oxidation pathway increased isoprene SOA mass concentrations in the southeastern United States by about 30%, increases of 0.4 to 0.6 μg m^{-3}. The larger NO_3 + isoprene SOA mass yields suggested in this paper, with average value of 30%, could double this expected NO_3 radical enhancement of SOA production. Edwards et al. (2017) concluded that the southeast U.S. is currently in transition between NO_x-independent and NO_x-controlled nighttime BVOC oxidation regime. If NO_3-isoprene oxidation is a larger aerosol source than currently understood, and if future NO_x reductions lead to a stronger sensitivity in nighttime BVOC oxidation rates, regional SOA loadings could decrease by a substantial fraction from the typical regional summertime OA loadings of 5 +/- 3 μg m^{-3} (Saha et al., 2017).

Analysis of the degree of oxidation and chemical composition of NO_3 + isoprene SOA would help to elucidate mechanistic reasons for the different field and lab SOA yields. For example, the potential contribution of the uptake of morning-after OH + NISOPOOH produced epoxides, discussed above in section 4.3, onto existing (acidic) aerosol could be quantified by measurement of these intermediates or their products in the aerosol phase. Assessment of degree of oxidation could help determine whether auto-oxidation mechanisms are active. Future

similar field studies would benefit from the co-deployment of the complementary tool of a Chemical Ionization Mass Spectrometer (CIMS) to detect NO_3 + isoprene products such as organic nitrates (Slade et al., 2017;Lee et al., 2016). Because of the potentially large effect on predicted SOA loading in regions of high isoprene emissions, a better mechanistic understanding of these observed yields is crucial.

Acknowledgements

JLF gratefully acknowledges funding from the EPA STAR Program (no. RD-83539901) and from the Fulbright U.S. Scholars Program in the Netherlands. PCJ, DAD, and JLJ were partially supported by EPA STAR 83587701-0 and DOE (BER/ASR) DE-SC0016559. This paper has not been formally reviewed by EPA. The views expressed in this document are solely those of the authors, and do not necessarily reflect those of EPA. EPA does not endorse any products or commercial services mentioned in this publication.

5 References

Allan, J. D., Bower, K. N., Coe, H., Boudries, H., Jayne, J. T., Canagaratna, M. R., Millet, D. B., Goldstein, A. H., Quinn, P. K., Weber, R. J., and Worsnop, D. R.: Submicron aerosol composition at Trinidad Head, California, during ITCT 2K2: Its relationship with gas phase volatile organic carbon and assessment of instrument performance, Journal of Geophysical Research: Atmospheres, 109, n/a-n/a, 10.1029/2003JD004208, 2004a.

Allan, J. D., Delia, A. E., Coe, H., Bower, K. N., Alfarra, M. R., Jimenez, J. L., Middlebrook, A. M., Drewnick, F., Onasch, T. B., Canagaratna, M. R., Jayne, J. T., and Worsnop, D. R.: A generalised method for the extraction of chemically resolved mass spectra from Aerodyne aerosol mass spectrometer data, Journal of Aerosol Science, 35, 909-922, 2004b.

Atkinson, R., Baulch, D. L., Cox, R. A., Crowley, J. N., Hampson, R. F., Hynes, R. G., Jenkin, M. E., Rossi, M. J., and Troe, J.: Evaluated kinetic and photochemical data for atmospheric chemistry: Volume I - gas phase reactions of Ox, HOx, NOx and SOx species, Atmos. Chem. Phys., 4, 1461-1738, 10.5194/acp-4-1461-2004, 2004.

Ayres, B. R., Allen, H. M., Draper, D. C., Brown, S. S., Wild, R. J., Jimenez, J. L., Day, D. A., Campuzano-Jost, P., Hu, W., de Gouw, J., Koss, A., Cohen, R. C., Duffey, K. C., Romer, P., Baumann, K., Edgerton, E., Takahama, S., Thornton, J. A., Lee, B. H., Lopez-Hilfiker, F. D., Mohr, C., Wennberg, P. O., Nguyen, T. B., Teng, A., Goldstein, A. H., Olson, K., and Fry, J. L.: Organic nitrate aerosol formation via NO₃ + biogenic volatile organic compounds in the southeastern United States, Atmos. Chem. Phys., 15, 13377-13392, 10.5194/acp-15-13377-2015, 2015.

Bahreini, R., Dunlea, E. J., Matthew, B. M., Simons, C., Docherty, K. S., DeCarlo, P. F., Jimenez, J. L., Brock, C. A., and Middlebrook, A. M.: Design and Operation of a Pressure-Controlled Inlet for Airborne Sampling with an Aerodynamic Aerosol Lens, Aerosol Science and Technology, 42, 465-471, 10.1080/02786820802178514, 2008.

Bahreini, R., Ervens, B., Middlebrook, A. M., Warneke, C., de Gouw, J. A., DeCarlo, P. F., Jimenez, J. L., Brock, C. A., Neuman, J. A., Ryerson, T. B., Stark, H., Atlas, E., Brioude, J., Fried, A., Holloway, J. S., Peischl, J., Richter, D., Walega, J., Weibring, P., Wollny, A. G., and Fehsenfeld, F. C.: Organic aerosol formation in urban and industrial plumes near Houston and Dallas, Texas, Journal of Geophysical Research: Atmospheres, 114, n/a-n/a, 10.1029/2008JD011493, 2009.

927 Boyd, C. M., Sanchez, J., Xu, L., Eugene, A. J., Nah, T., Tuet, W. Y., Guzman, M. I., and Ng, N.
928 L.: Secondary organic aerosol formation from the β-pinene+NO3 system: effect of humidity and
929 peroxy radical fate, Atmos. Chem. Phys., 15, 7497-7522, 10.5194/acp-15-7497-2015, 2015.

930 Brock, C. A., Cozic, J., Bahreini, R., Froyd, K. D., Middlebrook, A. M., McComiskey, A., Brioude,
931 J., Cooper, O. R., Stohl, A., Aikin, K. C., de Gouw, J. A., Fahey, D. W., Ferrare, R. A., Gao, R.
932 S., Gore, W., Holloway, J. S., Hübler, G., Jefferson, A., Lack, D. A., Lance, S., Moore, R. H.,
933 Murphy, D. M., Nenes, A., Novelli, P. C., Nowak, J. B., Ogren, J. A., Peischl, J., Pierce, R. B.,
934 Pilewskie, P., Quinn, P. K., Ryerson, T. B., Schmidt, K. S., Schwarz, J. P., Sodemann, H.,
935 Spackman, J. R., Stark, H., Thomson, D. S., Thornberry, T., Veres, P., Watts, L. A., Warneke,
936 C., and Wollny, A. G.: Characteristics, sources, and transport of aerosols measured in spring
937 2008 during the aerosol, radiation, and cloud processes affecting Arctic Climate (ARCPAC)
938 Project, Atmos. Chem. Phys., 11, 2423-2453, 10.5194/acp-11-2423-2011, 2011.

939 Brock, C. A., Wagner, N. L., Anderson, B. E., Attwood, A. R., Beyersdorf, A., Campuzano-Jost,
940 P., Carlton, A. G., Day, D. A., Diskin, G. S., Gordon, T. D., Jimenez, J. L., Lack, D. A., Liao, J.,
941 Markovic, M. Z., Middlebrook, A. M., Ng, N. L., Perring, A. E., Richardson, M. S., Schwarz, J. P.,
942 Washenfelder, R. A., Welti, A., Xu, L., Ziemba, L. D., and Murphy, D. M.: Aerosol optical
943 properties in the southeastern United States in summer – Part 1: Hygroscopic growth, Atmos.
944 Chem. Phys., 16, 4987-5007, 10.5194/acp-16-4987-2016, 2016.

945 Brown, S. S., Neuman, J. A., Ryerson, T. B., Trainer, M., Dubé, W. P., Holloway, J. S.,
946 Warneke, C., de Gouw, J. A., Donnelly, S. G., Atlas, E., Matthew, B., Middlebrook, A. M.,
947 Peltier, R., Weber, R. J., Stohl, A., Meagher, J. F., Fehsenfeld, F. C., and Ravishankara, A. R.:
948 Nocturnal odd-oxygen budget and its implications for ozone loss in the lower troposphere,
949 Geophysical Research Letters, 33, n/a-n/a, 10.1029/2006GL025900, 2006.

950 Brown, S. S., deGouw, J. A., Warneke, C., Ryerson, T. B., Dubé, W. P., Atlas, E., Weber, R. J.,
951 Peltier, R. E., Neuman, J. A., Roberts, J. M., Swanson, A., Flocke, F., McKeen, S. A., Brioude,
952 J., Sommariva, R., Trainer, M., Fehsenfeld, F. C., and Ravishankara, A. R.: Nocturnal isoprene
953 oxidation over the Northeast United States in summer and its impact on reactive nitrogen
954 partitioning and secondary organic aerosol, Atmos. Chem. Phys., 9, 3027-3042, 10.5194/acp-9-
955 3027-2009, 2009.

956 Brown, S. S., Dubé, W. P., Karamchandani, P., Yarwood, G., Peischl, J., Ryerson, T. B.,
957 Neuman, J. A., Nowak, J. B., Holloway, J. S., Washenfelder, R. A., Brock, C. A., Frost, G. J.,
958 Trainer, M., Parrish, D. D., Fehsenfeld, F. C., and Ravishankara, A. R.: Effects of NOxcontrol
959 and plume mixing on nighttime chemical processing of plumes from coal-fired power plants,
960 Journal of Geophysical Research: Atmospheres, 117, n/a-n/a, 10.1029/2011JD016954, 2012.

961 Brown, S. S., and Stutz, J.: Nighttime radical observations and chemistry, Chemical Society
962 Reviews, 41, 6405-6447, 10.1039/C2CS35181A, 2012.

963 Brown, S. S., Dubé, W. P., Bahreini, R., Middlebrook, A. M., Brock, C. A., Warneke, C., de
964 Gouw, J. A., Washenfelder, R. A., Atlas, E., Peischl, J., Ryerson, T. B., Holloway, J. S.,
965 Schwarz, J. P., Spackman, R., Trainer, M., Parrish, D. D., Fehshenfeld, F. C., and
966 Ravishankara, A. R.: Biogenic VOC oxidation and organic aerosol formation in an urban
967 nocturnal boundary layer: aircraft vertical profiles in Houston, TX, Atmos. Chem. Phys., 13,
968 11317-11337, 10.5194/acp-13-11317-2013, 2013.

969 Bruns, E. A., Perraud, V., Zelenyuk, A., Ezell, M. J., Johnson, S. N., Yu, Y., Imre, D., Finlayson-
970 Pitts, B. J., and Alexander, M. L.: Comparison of FTIR and Particle Mass Spectrometry for the
971 Measurement of Particulate Organic Nitrates, Environmental Science & Technology, 44, 1056-
972 1061, 2010.

973 Cai, Y., C. Montague, D., Mooiweer-Bryan, W., and Deshler, T.: Performance characteristics of
974 the ultra high sensitivity aerosol spectrometer for particles between 55 and 800 nm: Laboratory
975 and field studies, 759-769 pp., 2008.

976 Calvert, J. G., Atkinson, J. A., Kerr, J. A., Madronich, S., Moortgat, G. K., Wallington, T. J., and
977 Yarwood, G.: Mechanisms of the atmospheric oxidation of the alkenes, Oxford University Press,
978 New York, NY, 2000.

979 Carlton, A. G., Wiedinmyer, C., and Kroll, J. H.: A review of Secondary Organic Aerosol (SOA)
980 formation from isoprene, Atmos. Chem. Phys., 9, 4987-5005, 10.5194/acp-9-4987-2009, 2009.

981 Carlton, A. G., Pinder, R. W., Bhave, P. V., and Pouliot, G. A.: To What Extent Can Biogenic
982 SOA be Controlled?, Environmental Science & Technology, 44, 3376-3380,
983 10.1021/es903506b, 2010.

984 Crounse, J. D., Paulot, F., Kjaergaard, H. G., and Wennberg, P. O.: Peroxy radical
985 isomerization in the oxidation of isoprene, Physical Chemistry Chemical Physics, 13, 13607-
986 13613, 10.1039/C1CP21330J, 2011.

987 D'Ambro, E. L., Møller, K. H., Lopez-Hilfiker, F. D., Schobesberger, S., Liu, J., Shilling, J. E.,
988 Lee, B. H., Kjaergaard, H. G., and Thornton, J. A.: Isomerization of Second-Generation
989 Isoprene Peroxy Radicals: Epoxide Formation and Implications for Secondary Organic Aerosol
990 Yields, Environmental Science & Technology, 51, 4978-4987, 10.1021/acs.est.7b00460, 2017.

991 Darer, A. I., Cole-Filipiak, N. C., O'Connor, A. E., and Elrod, M. J.: Formation and Stability of
992 Atmospherically Relevant Isoprene-Derived Organosulfates and Organonitrates, Environmental
993 Science & Technology, 45, 1895-1902, 10.1021/es103797z, 2011.

994 Day, D. A., Campuzano-Jost, P., Palm, B. B., Hu, W. W., Nault, B. A., Wooldridge, P. J., Cohen,
995 R. C., Docherty, K. S., Huffman, J. A., and Jimenez, J. L.: Evaluation of methods for
996 quantification of bulk particle-phase organic nitrates using real-time aerosol mass spectrometry,
997 in preparation, 2017.

998 Dommen, J., Hellén, H., Saurer, M., Jaeggi, M., Siegwolf, R., Metzger, A., Duplissy, J., Fierz,
999 M., and Baltensperger, U.: Determination of the Aerosol Yield of Isoprene in the Presence of an
1000 Organic Seed with Carbon Isotope Analysis, Environmental Science & Technology, 43, 6697-
1001 6702, 10.1021/es9006959, 2009.

1002 Drewnick, F., Hings, S. S., DeCarlo, P., Jayne, J. T., Gonin, M., Fuhrer, K., Weimer, S.,
1003 Jimenez, J. L., Demerjian, K. L., Borrmann, S., and Worsnop, D. R.: A New Time-of-Flight
1004 Aerosol Mass Spectrometer (TOF-AMS)—Instrument Description and First Field Deployment,
1005 Aerosol Science and Technology, 39, 637-658, 10.1080/02786820500182040, 2005.

1006 Dunlea, E. J., DeCarlo, P. F., Aiken, A. C., Kimmel, J. R., Peltier, R. E., Weber, R. J.,
1007 Tomlinson, J., Collins, D. R., Shinozuka, Y., McNaughton, C. S., Howell, S. G., Clarke, A. D.,
1008 Emmons, L. K., Apel, E. C., Pfister, G. G., van Donkelaar, A., Martin, R. V., Millet, D. B., Heald,
1009 C. L., and Jimenez, J. L.: Evolution of Asian aerosols during transpacific transport in INTEX-B,
1010 Atmos. Chem. Phys., 9, 7257-7287, 10.5194/acp-9-7257-2009, 2009.

1011 Edwards, P. M., Aikin, K. C., Dube, W. P., Fry, J. L., Gilman, J. B., de Gouw, J. A., Graus, M.
1012 G., Hanisco, T. F., Holloway, J., Hubler, G., Kaiser, J., Keutsch, F. N., Lerner, B. M., Neuman, J.
1013 A., Parrish, D. D., Peischl, J., Pollack, I. B., Ravishankara, A. R., Roberts, J. M., Ryerson, T. B.,
1014 Trainer, M., Veres, P. R., Wolfe, G. M., Warneke, C., and Brown, S. S.: Transition from high- to
1015 low-NOx control of night-time oxidation in the southeastern US, Nature Geosci, 10, 490-495,
1016 10.1038/ngeo2976

http://www.nature.com/ngeo/journal/v10/n7/abs/ngeo2976.html - supplementary-information, 2017.

Ehn, M., Thornton, J. A., Kleist, E., Sipila, M., Junninen, H., Pullinen, I., Springer, M., Rubach, F., Tillmann, R., Lee, B., Lopez-Hilfiker, F., Andres, S., Acir, I.-H., Rissanen, M., Jokinen, T., Schobesberger, S., Kangasluoma, J., Kontkanen, J., Nieminen, T., Kurten, T., Nielsen, L. B., Jorgensen, S., Kjaergaard, H. G., Canagaratna, M., Maso, M. D., Berndt, T., Petaja, T., Wahner, A., Kerminen, V.-M., Kulmala, M., Worsnop, D. R., Wildt, J., and Mentel, T. F.: A large source of low-volatility secondary organic aerosol, Nature, 506, 476-479, 10.1038/nature13032, 2014.

Emmerson, K. M., and Evans, M. J.: Comparison of tropospheric gas-phase chemistry schemes for use within global models, Atmos. Chem. Phys., 9, 1831-1845, 10.5194/acp-9-1831-2009, 2009.

Farmer, D. K., Matsunaga, A., Docherty, K. S., Surratt, J. D., Seinfeld, J. H., Ziemann, P. J., and Jimenez, J. L.: Response of an aerosol mass spectrometer to organonitrates and organosulfates and implications for atmospheric chemistry, Proceedings of the National Academy of Sciences, 107, 6670-6675, 2010.

Fisher, J. A., Jacob, D. J., Travis, K. R., Kim, P. S., Marais, E. A., Chan Miller, C., Yu, K., Zhu, L., Yantosca, R. M., Sulprizio, M. P., Mao, J., Wennberg, P. O., Crounse, J. D., Teng, A. P., Nguyen, T. B., St. Clair, J. M., Cohen, R. C., Romer, P., Nault, B. A., Wooldridge, P. J., Jimenez, J. L., Campuzano-Jost, P., Day, D. A., Hu, W., Shepson, P. B., Xiong, F., Blake, D. R., Goldstein, A. H., Misztal, P. K., Hanisco, T. F., Wolfe, G. M., Ryerson, T. B., Wisthaler, A., and Mikoviny, T.: Organic nitrate chemistry and its implications for nitrogen budgets in an isoprene- and monoterpene-rich atmosphere: constraints from aircraft (SEAC4RS) and ground-based (SOAS) observations in the Southeast US, Atmos. Chem. Phys., 16, 5969-5991, 10.5194/acp-16-5969-2016, 2016.

Fry, J. L., Kiendler-Scharr, A., Rollins, A. W., Wooldridge, P. J., Brown, S. S., Fuchs, H., Dube, W., Mensah, A., dal Maso, M., Tillmann, R., Dorn, H. P., Brauers, T., and Cohen, R. C.: Organic nitrate and secondary organic aerosol yield from NO3 oxidation of beta-pinene evaluated using a gas-phase kinetics/aerosol partitioning model, Atmospheric Chemistry and Physics, 9, 1431-1449, 2009.

Fry, J. L., Kiendler-Scharr, A., Rollins, A. W., Brauers, T., Brown, S. S., Dorn, H.-P., Dube, W. P., Fuchs, H., Mensah, A., Rohrer, F., Tillmann, R., Wahner, A., Wooldridge, P. J., and Cohen, R. C.: SOA from limonene: role of NO3 in its generation and degradation, Atmospheric Chemistry and Physics, 11, 3879-3894, 2011.

Fry, J. L., Draper, D. C., Zarzana, K. J., Campuzano-Jost, P., Day, D. A., Jimenez, J. L., Brown, S. S., Cohen, R. C., Kaser, L., Hansel, A., Cappellin, L., Karl, T., Hodzic Roux, A., Turnipseed, A., Cantrell, C., Lefer, B. L., and Grossberg, N.: Observations of gas- and aerosol-phase organic nitrates at BEACHON-RoMBAS 2011, Atmos. Chem. Phys., 13, 8585-8605, 10.5194/acp-13-8585-2013, 2013.

Fry, J. L., Koski, C., Bott, K., Hsu-Flanders, R., and Hazell, M.: Downwind particulate matters: Regulatory implications of secondary aerosol formation from the interaction of nitrogen oxides and tree emissions, Environmental Science & Policy, 50, 180-190, http://dx.doi.org/10.1016/j.envsci.2015.02.017, 2015.

Goldstein, A. H., Koven, C. D., Heald, C. L., and Fung, I. Y.: Biogenic carbon and anthropogenic pollutants combine to form a cooling haze over the southeastern United States, Proceedings of the National Academy of Sciences, 106, 8835-8840, 10.1073/pnas.0904128106, 2009.

1063 Guenther, A., Karl, T., Harley, P., Wiedinmyer, C., Palmer, P. I., and Geron, C.: Estimates of
1064 global terrestrial isoprene emissions using MEGAN (Model of Emissions of Gases and Aerosols
1065 from Nature), Atmos. Chem. Phys, 6, 3181-3210, 2006.

1066 Guo, H., Xu, L., Bougiatioti, A., Cerully, K. M., Capps, S. L., Hite Jr, J. R., Carlton, A. G., Lee, S.
1067 H., Bergin, M. H., Ng, N. L., Nenes, A., and Weber, R. J.: Fine-particle water and pH in the
1068 southeastern United States, Atmos. Chem. Phys., 15, 5211-5228, 10.5194/acp-15-5211-2015,
1069 2015.

1070 Hallquist, M., Wenger, J. C., Baltensperger, U., Rudich, Y., Simpson, D., Claeys, M., Dommen,
1071 J., Donahue, N. M., George, C., Goldstein, A. H., Hamilton, J. F., Herrmann, H., Hoffmann, T.,
1072 Iinuma, Y., Jang, M., Jenkin, M. E., Jimenez, J. L., Kiendler-Scharr, A., Maenhaut, W.,
1073 McFiggans, G., Mentel, T. F., Monod, A., Prévôt, A. S. H., Seinfeld, J. H., Surratt, J. D.,
1074 Szmigielski, R., and Wildt, J.: The formation, properties and impact of secondary organic
1075 aerosol: current and emerging issues, Atmospheric Chemistry & Physics, 9, 5155-5235, 2009.

1076 Hayes, P. L., Ortega, A. M., Cubison, M. J., Froyd, K. D., Zhao, Y., Cliff, S. S., Hu, W. W.,
1077 Toohey, D. W., Flynn, J. H., Lefer, B. L., Grossberg, N., Alvarez, S., Rappenglück, B., Taylor, J.
1078 W., Allan, J. D., Holloway, J. S., Gilman, J. B., Kuster, W. C., de Gouw, J. A., Massoli, P.,
1079 Zhang, X., Liu, J., Weber, R. J., Corrigan, A. L., Russell, L. M., Isaacman, G., Worton, D. R.,
1080 Kreisberg, N. M., Goldstein, A. H., Thalman, R., Waxman, E. M., Volkamer, R., Lin, Y. H.,
1081 Surratt, J. D., Kleindienst, T. E., Offenberg, J. H., Dusanter, S., Griffith, S., Stevens, P. S.,
1082 Brioude, J., Angevine, W. M., and Jimenez, J. L.: Organic aerosol composition and sources in
1083 Pasadena, California, during the 2010 CalNex campaign, Journal of Geophysical Research:
1084 Atmospheres, 118, 9233-9257, 10.1002/jgrd.50530, 2013.

1085 Heald, C. L., Henze, D. K., Horowitz, L. W., Feddema, J., Lamarque, J. F., Guenther, A., Hess,
1086 P. G., Vitt, F., Seinfeld, J. H., Goldstein, A. H., and Fung, I.: Predicted change in global
1087 secondary organic aerosol concentrations in response to future climate, emissions, and land
1088 use change, Journal of Geophysical Research: Atmospheres, 113, n/a-n/a,
1089 10.1029/2007JD009092, 2008.

1090 Henze, D. K., and Seinfeld, J. H.: Global secondary organic aerosol from isoprene oxidation,
1091 Geophysical Research Letters, 33, Artn L09812

1092 Doi 10.1029/2006gl025976, 2006.

1093 Hoyle, C., Boy, M., Donahue, N., Fry, J., Glasius, M., Guenther, A., Hallar, A., Hartz, K. H.,
1094 Petters, M., and Petaja, T.: A review of the anthropogenic influence on biogenic secondary
1095 organic aerosol, Atmospheric Chemistry and Physics, 11, 321-343, 2011.

1096 Hoyle, C. R., Berntsen, T., Myhre, G., and Isaksen, I. S. A.: Secondary organic aerosol in the
1097 global aerosol - chemical transport model Oslo CTM2, Atmospheric Chemistry and Physics, 7,
1098 5675-5694, 2007.

1099 Hu, K. S., Darer, A. I., and Elrod, M. J.: Thermodynamics and kinetics of the hydrolysis of
1100 atmospherically relevant organonitrates and organosulfates, Atmos. Chem. Phys., 11, 8307-
1101 8320, 10.5194/acp-11-8307-2011, 2011.

1102 Hu, W. W., Campuzano-Jost, P., Palm, B. B., Day, D. A., Ortega, A. M., Hayes, P. L., Krechmer,
1103 J. E., Chen, Q., Kuwata, M., Liu, Y. J., de Sá, S. S., McKinney, K., Martin, S. T., Hu, M.,
1104 Budisulistiorini, S. H., Riva, M., Surratt, J. D., St. Clair, J. M., Isaacman-Van Wertz, G., Yee, L.
1105 D., Goldstein, A. H., Carbone, S., Brito, J., Artaxo, P., de Gouw, J. A., Koss, A., Wisthaler, A.,
1106 Mikoviny, T., Karl, T., Kaser, L., Jud, W., Hansel, A., Docherty, K. S., Alexander, M. L.,
1107 Robinson, N. H., Coe, H., Allan, J. D., Canagaratna, M. R., Paulot, F., and Jimenez, J. L.:
1108 Characterization of a real-time tracer for isoprene epoxydiols-derived secondary organic aerosol

(IEPOX-SOA) from aerosol mass spectrometer measurements, Atmos. Chem. Phys., 15, 11807-11833, 10.5194/acp-15-11807-2015, 2015.

Jenkin, M. E., Young, J. C., and Rickard, A. R.: The MCM v3.3.1 degradation scheme for isoprene, Atmos. Chem. Phys., 15, 11433-11459, 10.5194/acp-15-11433-2015, 2015.

Jimenez, J. L., Canagaratna, M. R., Donahue, N. M., Prevot, A. S. H., Zhang, Q., Kroll, J. H., DeCarlo, P. F., Allan, J. D., Coe, H., Ng, N. L., Aiken, A. C., Docherty, K. S., Ulbrich, I. M., Grieshop, A. P., Robinson, A. L., Duplissy, J., Smith, J. D., Wilson, K. R., Lanz, V. A., Hueglin, C., Sun, Y. L., Tian, J., Laaksonen, A., Raatikainen, T., Rautiainen, J., Vaattovaara, P., Ehn, M., Kulmala, M., Tomlinson, J. M., Collins, D. R., Cubison, M. J., E., Dunlea, J., Huffman, J. A., Onasch, T. B., Alfarra, M. R., Williams, P. I., Bower, K., Kondo, Y., Schneider, J., Drewnick, F., Borrmann, S., Weimer, S., Demerjian, K., Salcedo, D., Cottrell, L., Griffin, R., Takami, A., Miyoshi, T., Hatakeyama, S., Shimono, A., Sun, J. Y., Zhang, Y. M., Dzepina, K., Kimmel, J. R., Sueper, D., Jayne, J. T., Herndon, S. C., Trimborn, A. M., Williams, L. R., Wood, E. C., Middlebrook, A. M., Kolb, C. E., Baltensperger, U., and Worsnop, D. R.: Evolution of Organic Aerosols in the Atmosphere, Science, 1525-1529, 2009.

Kanakidou, M., Seinfeld, J. H., Pandis, S. N., Barnes, I., Dentener, F. J., Facchini, M. C., Van Dingenen, R., Ervens, B., Nenes, A., Nielsen, C. J., Swietlicki, E., Putaud, J. P., Balkanski, Y., Fuzzi, S., Horth, J., Moortgat, G. K., Winterhalter, R., Myhre, C. E. L., Tsigaridis, K., Vignati, E., Stephanou, E. G., and Wilson, J.: Organic aerosol and global climate modelling: a review, Atmospheric Chemistry and Physics, 5, 1053-1123, 2005.

Kiendler-Scharr, A., Mensah, A. A., Friese, E., Topping, D., Nemitz, E., Prevot, A. S. H., Äijälä, M., Allan, J., Canonaco, F., Canagaratna, M., Carbone, S., Crippa, M., Dall Osto, M., Day, D. A., De Carlo, P., Di Marco, C. F., Elbern, H., Eriksson, A., Freney, E., Hao, L., Herrmann, H., Hildebrandt, L., Hillamo, R., Jimenez, J. L., Laaksonen, A., McFiggans, G., Mohr, C., O'Dowd, C., Otjes, R., Ovadnevaite, J., Pandis, S. N., Poulain, L., Schlag, P., Sellegri, K., Swietlicki, E., Tiitta, P., Vermeulen, A., Wahner, A., Worsnop, D., and Wu, H. C.: Ubiquity of organic nitrates from nighttime chemistry in the European submicron aerosol, Geophysical Research Letters, 43, 7735-7744, 10.1002/2016GL069239, 2016.

Kim, P. S., Jacob, D. J., Fisher, J. A., Travis, K., Yu, K., Zhu, L., Yantosca, R. M., Sulprizio, M. P., Jimenez, J. L., Campuzano-Jost, P., Froyd, K. D., Liao, J., Hair, J. W., Fenn, M. A., Butler, C. F., Wagner, N. L., Gordon, T. D., Welti, A., Wennberg, P. O., Crounse, J. D., St. Clair, J. M., Teng, A. P., Millet, D. B., Schwarz, J. P., Markovic, M. Z., and Perring, A. E.: Sources, seasonality, and trends of southeast US aerosol: an integrated analysis of surface, aircraft, and satellite observations with the GEOS-Chem chemical transport model, Atmos. Chem. Phys., 15, 10411-10433, 10.5194/acp-15-10411-2015, 2015.

Kleindienst, T. E., Lewandowski, M., Offenberg, J. H., Jaoui, M., and Edney, E. O.: Ozone-isoprene reaction: Re-examination of the formation of secondary organic aerosol, Geophysical Research Letters, 34, n/a-n/a, 10.1029/2006GL027485, 2007.

Krechmer, J. E., Pagonis, D., Ziemann, P. J., and Jimenez, J. L.: Quantification of Gas-Wall Partitioning in Teflon Environmental Chambers Using Rapid Bursts of Low-Volatility Oxidized Species Generated in Situ, Environmental Science & Technology, 50, 5757-5765, 10.1021/acs.est.6b00606, 2016.

Kroll, J. H., Ng, N. L., Murphy, S. M., Flagan, R. C., and Seinfeld, J. H.: Secondary Organic Aerosol Formation from Isoprene Photooxidation, Environmental Science & Technology, 40, 1869-1877, 10.1021/es0524301, 2006.

Kurtén, T., Møller, K. H., Nguyen, T. B., Schwantes, R. H., Misztal, P. K., Su, L., Wennberg, P. O., Fry, J. L., and Kjaergaard, H. G.: Alkoxy Radical Bond Scissions Explain the Anomalously Low Secondary Organic Aerosol and Organonitrate Yields From α-Pinene + NO3, The Journal of Physical Chemistry Letters, 2826-2834, 10.1021/acs.jpclett.7b01038, 2017.

Lee, B. H., Mohr, C., Lopez-Hilfiker, F. D., Lutz, A., Hallquist, M., Lee, L., Romer, P., Cohen, R. C., Iyer, S., Kurtén, T., Hu, W., Day, D. A., Campuzano-Jost, P., Jimenez, J. L., Xu, L., Ng, N. L., Guo, H., Weber, R. J., Wild, R. J., Brown, S. S., Koss, A., de Gouw, J., Olson, K., Goldstein, A. H., Seco, R., Kim, S., McAvey, K., Shepson, P. B., Starn, T., Baumann, K., Edgerton, E. S., Liu, J., Shilling, J. E., Miller, D. O., Brune, W., Schobesberger, S., D'Ambro, E. L., and Thornton, J. A.: Highly functionalized organic nitrates in the southeast United States: Contribution to secondary organic aerosol and reactive nitrogen budgets, Proceedings of the National Academy of Sciences, 113, 1516-1521, 2016.

Lelieveld, J., Evans, J. S., Fnais, M., Giannadaki, D., and Pozzer, A.: The contribution of outdoor air pollution sources to premature mortality on a global scale, Nature, 525, 367-371, 10.1038/nature15371, 2015.

Lerner, B. M., Gilman, J. B., Aikin, K. C., Atlas, E. L., Goldan, P. D., Graus, M., Hendershot, R., Isaacman-VanWertz, G. A., Koss, A., Kuster, W. C., Lueb, R. A., McLaughlin, R. J., Peischl, J., Sueper, D., Ryerson, T. B., Tokarek, T. W., Warneke, C., Yuan, B., and de Gouw, J. A.: An improved, automated whole air sampler and gas chromatography mass spectrometry analysis system for volatile organic compounds in the atmosphere, Atmos. Meas. Tech., 10, 291-313, 10.5194/amt-10-291-2017, 2017.

Liu, J., D'Ambro, E. L., Lee, B. H., Lopez-Hilfiker, F. D., Zaveri, R. A., Rivera-Rios, J. C., Keutsch, F. N., Iyer, S., Kurten, T., Zhang, Z., Gold, A., Surratt, J. D., Shilling, J. E., and Thornton, J. A.: Efficient Isoprene Secondary Organic Aerosol Formation from a Non-IEPOX Pathway, Environmental Science & Technology, 50, 9872-9880, 10.1021/acs.est.6b01872, 2016.

Marais, E. A., Jacob, D. J., Jimenez, J. L., Campuzano-Jost, P., Day, D. A., Hu, W., Krechmer, J., Zhu, L., Kim, P. S., Miller, C. C., Fisher, J. A., Travis, K., Yu, K., Hanisco, T. F., Wolfe, G. M., Arkinson, H. L., Pye, H. O. T., Froyd, K. D., Liao, J., and McNeill, V. F.: Aqueous-phase mechanism for secondary organic aerosol formation from isoprene: application to the southeast United States and co-benefit of SO2 emission controls, Atmos. Chem. Phys., 16, 1603-1618, 10.5194/acp-16-1603-2016, 2016.

Marcolli, C., Canagaratna, M. R., Worsnop, D. R., Bahreini, R., de Gouw, J. A., Warneke, C., Goldan, P. D., Kuster, W. C., Williams, E. J., Lerner, B. M., Roberts, J. M., Meagher, J. F., Fehsenfeld, F. C., Marchewka, M., Bertman, S. B., and Middlebrook, A. M.: Cluster Analysis of the Organic Peaks in Bulk Mass Spectra Obtained During the 2002 New England Air Quality Study with an Aerodyne Aerosol Mass Spectrometer, Atmos. Chem. Phys., 6, 5649-5666, 10.5194/acp-6-5649-2006, 2006.

Matsunaga, A., and Ziemann, P. J.: Gas-Wall Partitioning of Organic Compounds in a Teflon Film Chamber and Potential Effects on Reaction Product and Aerosol Yield Measurements, Aerosol Science and Technology, 44, 881-892, 10.1080/02786826.2010.501044, 2010.

Middlebrook, A. M., Bahreini, R., Jimenez, J. L., and Canagaratna, M. R.: Evaluation of Composition-Dependent Collection Efficiencies for the Aerodyne Aerosol Mass Spectrometer using Field Data, Aerosol Science and Technology, 46, 258-271, 10.1080/02786826.2011.620041, 2012.

Myhre, G., Shindell, D., Bréon, F.-M., Collins, W., Fuglestvedt, J., Huang, J., Koch, D., Lamarque, J.-F., Lee, D., Mendoza, B., Nakajima, T., Robock, A., Stephens, G., Takemura, T., and Zhang, H.: Anthropogenic And Natural Radiative Forcing, in Climate Change 2013: The Physical Science Basis. Contribution of Working Group I to the Fifth Assessment Report of the Intergovernmental Panel on Climate Change, in, edited by: Stocker, T. F., Qin, D., Plattner, G.-K., Tignor, M., Allen, S. K., Boschung, J., Nauels, A., Xia, Y., Bex, V., and Midgley, P. M., Cambridge University Press, New York, NY, USA, 659-740, 2013.

Ng, N. L., Kwan, A. J., Surratt, J. D., Chan, A. W. H., Chhabra, P. S., Sorooshian, A., Pye, H. O. T., Crounse, J. D., Wennberg, P. O., Flagan, R. C., and Seinfeld, J. H.: Secondary organic aerosol (SOA) formation from reaction of isoprene with nitrate radicals (NO3), Atmos. Chem. Phys., 8, 4117-4140, 2008.

Ng, N. L., Brown, S. S., Archibald, A. T., Atlas, E., Cohen, R. C., Crowley, J. N., Day, D. A., Donahue, N. M., Fry, J. L., Fuchs, H., Griffin, R. J., Guzman, M. I., Herrmann, H., Hodzic, A., Iinuma, Y., Jimenez, J. L., Kiendler-Scharr, A., Lee, B. H., Luecken, D. J., Mao, J., McLaren, R., Mutzel, A., Osthoff, H. D., Ouyang, B., Picquet-Varrault, B., Platt, U., Pye, H. O. T., Rudich, Y., Schwantes, R. H., Shiraiwa, M., Stutz, J., Thornton, J. A., Tilgner, A., Williams, B. J., and Zaveri, R. A.: Nitrate radicals and biogenic volatile organic compounds: oxidation, mechanisms, and organic aerosol, Atmos. Chem. Phys., 17, 2103-2162, 10.5194/acp-17-2103-2017, 2017.

Palm, B. B., Campuzano-Jost, P., Day, D. A., Ortega, A. M., Fry, J. L., Brown, S. S., Zarzana, K. J., Dube, W., Wagner, N. L., Draper, D. C., Kaser, L., Jud, W., Karl, T., Hansel, A., Gutiérrez-Montes, C., and Jimenez, J. L.: Secondary organic aerosol formation from in situ OH, O3, and NO3 oxidation of ambient forest air in an oxidation flow reactor, Atmos. Chem. Phys., 17, 5331-5354, 10.5194/acp-17-5331-2017, 2017.

Pankow, J. F., and Asher, W. E.: SIMPOL.1: a simple group contribution method for predicting vapor pressures and enthalpies of vaporization of multifunctional organic compounds, Atmospheric Chemistry and Physics, 8, 2773-2796, 10.5194/acp-8-2773-2008

, 2008.

Peischl, J., Ryerson, T. B., Holloway, J. S., Parrish, D. D., Trainer, M., Frost, G. J., Aikin, K. C., Brown, S. S., Dubé, W. P., Stark, H., and Fehsenfeld, F. C.: A top-down analysis of emissions from selected Texas power plants during TexAQS 2000 and 2006, Journal of Geophysical Research: Atmospheres, 115, n/a-n/a, 10.1029/2009JD013527, 2010.

Pye, H., Chan, A., Barkley, M., and Seinfeld, J.: Global modeling of organic aerosol: the importance of reactive nitrogen (NO_x and NO_3), Atmospheric Chemistry and Physics, 10, 11261-11276, 2010.

Pye, H. O. T., Luecken, D. J., Xu, L., Boyd, C. M., Ng, N. L., Baker, K. R., Ayres, B. R., Bash, J. O., Baumann, K., Carter, W. P. L., Edgerton, E., Fry, J. L., Hutzell, W. T., Schwede, D. B., and Shepson, P. B.: Modeling the Current and Future Roles of Particulate Organic Nitrates in the Southeastern United States, Environmental Science & Technology, 49, 14195-14203, 10.1021/acs.est.5b03738, 2015.

Rollins, A. W., Kiendler-Scharr, A., Fry, J. L., Brauers, T., Brown, S. S., Dorn, H.-P., Dube, W. P., Fuchs, H., Mensah, A., Mentel, T. F., Rohrer, F., Tillmann, R., Wegener, R., Wooldridge, P. J., and Cohen, R. C.: Isoprene oxidation by nitrate radical: alkyl nitrate and secondary organic aerosol yields, Atmos. Chem. Phys., 9, 6685-6703, 2009.

Rollins, A. W., Browne, E. C., Min, K. E., Pusede, S. E., Wooldridge, P. J., Gentner, D. R., Goldstein, A. H., Liu, S., Day, D. A., Russell, L. M., and Cohen, R. C.: Evidence for NOx Control over Nighttime SOA Formation, Science, 337, 1210, 2012.

1245 Romer, P. S., Duffey, K. C., Wooldridge, P. J., Allen, H. M., Ayres, B. R., Brown, S. S., Brune,
1246 W. H., Crounse, J. D., de Gouw, J., Draper, D. C., Feiner, P. A., Fry, J. L., Goldstein, A. H.,
1247 Koss, A., Misztal, P. K., Nguyen, T. B., Olson, K., Teng, A. P., Wennberg, P. O., Wild, R. J.,
1248 Zhang, L., and Cohen, R. C.: The lifetime of nitrogen oxides in an isoprene-dominated forest,
1249 Atmos. Chem. Phys., 16, 7623-7637, 10.5194/acp-16-7623-2016, 2016.

1250 Saha, P. K., Khlystov, A., Yahya, K., Zhang, Y., Xu, L., Ng, N. L., and Grieshop, A. P.:
1251 Quantifying the volatility of organic aerosol in the southeastern US, Atmos. Chem. Phys., 17,
1252 501-520, 10.5194/acp-17-501-2017, 2017.

1253 Sato, K., Takami, A., Isozaki, T., Hikida, T., Shimono, A., and Imamura, T.: Mass spectrometric
1254 study of secondary organic aerosol formed from the photo-oxidation of aromatic hydrocarbons,
1255 Atmospheric Environment, 44, 1080-1087, https://doi.org/10.1016/j.atmosenv.2009.12.013,
1256 2010.

1257 Schwantes, R. H., Teng, A. P., Nguyen, T. B., Coggon, M. M., Crounse, J. D., St. Clair, J. M.,
1258 Zhang, X., Schilling, K. A., Seinfeld, J. H., and Wennberg, P. O.: Isoprene NO3 Oxidation
1259 Products from the RO2 + HO2 Pathway, The Journal of Physical Chemistry A, 119, 10158-
1260 10171, 10.1021/acs.jpca.5b06355, 2015.

1261 Slade, J. H., de Perre, C., Lee, L., and Shepson, P. B.: Nitrate radical oxidation of γ-terpinene:
1262 hydroxy nitrate, total organic nitrate, and secondary organic aerosol yields, Atmos. Chem.
1263 Phys., 17, 8635-8650, 10.5194/acp-17-8635-2017, 2017.

1264 Spracklen, D. V., Jimenez, J. L., Carslaw, K. S., Worsnop, D. R., Evans, M. J., Mann, G. W.,
1265 Zhang, Q., Canagaratna, M. R., Allan, J., Coe, H., McFiggans, G., Rap, A., and Forster, P.:
1266 Aerosol mass spectrometer constraint on the global secondary organic aerosol budget, Atmos.
1267 Chem. Phys., 11, 12109-12136, 10.5194/acp-11-12109-2011, 2011.

1268 Surratt, J. D., Chan, A. W. H., Eddingsaas, N. C., Chan, M. N., Loza, C. L., Kwan, A. J., Hersey,
1269 S. P., Flagan, R. C., Wennberg, P. O., and Seinfeld, J. H.: Reactive intermediates revealed in
1270 secondary organic aerosol formation from isoprene, Proceedings of the National Academy of
1271 Sciences, 107, 6640-6645, 2010.

1272 Takegawa, N., Miyakawa, T., Kawamura, K., and Kondo, Y.: Contribution of Selected
1273 Dicarboxylic and ω-Oxocarboxylic Acids in Ambient Aerosol to the m/z 44 Signal of an
1274 Aerodyne Aerosol Mass Spectrometer, Aerosol Science and Technology, 41, 418-437,
1275 10.1080/02786820701203215, 2007.

1276 Toon, O. B., Maring, H., Dibb, J., Ferrare, R., Jacob, D. J., Jensen, E. J., Luo, Z. J., Mace, G.
1277 G., Pan, L. L., Pfister, L., Rosenlof, K. H., Redemann, J., Reid, J. S., Singh, H. B., Thompson,
1278 A. M., Yokelson, R., Minnis, P., Chen, G., Jucks, K. W., and Pszenny, A.: Planning,
1279 implementation, and scientific goals of the Studies of Emissions and Atmospheric Composition,
1280 Clouds and Climate Coupling by Regional Surveys (SEAC4RS) field mission, Journal of
1281 Geophysical Research: Atmospheres, 121, 4967-5009, 10.1002/2015JD024297, 2016.

1282 Warneke, C., Trainer, M., de Gouw, J. A., Parrish, D. D., Fahey, D. W., Ravishankara, A. R.,
1283 Middlebrook, A. M., Brock, C. A., Roberts, J. M., Brown, S. S., Neuman, J. A., Lerner, B. M.,
1284 Lack, D., Law, D., Hübler, G., Pollack, I., Sjostedt, S., Ryerson, T. B., Gilman, J. B., Liao, J.,
1285 Holloway, J., Peischl, J., Nowak, J. B., Aikin, K. C., Min, K. E., Washenfelder, R. A., Graus, M.
1286 G., Richardson, M., Markovic, M. Z., Wagner, N. L., Welti, A., Veres, P. R., Edwards, P.,
1287 Schwarz, J. P., Gordon, T., Dube, W. P., McKeen, S. A., Brioude, J., Ahmadov, R., Bougiatioti,
1288 A., Lin, J. J., Nenes, A., Wolfe, G. M., Hanisco, T. F., Lee, B. H., Lopez-Hilfiker, F. D., Thornton,
1289 J. A., Keutsch, F. N., Kaiser, J., Mao, J., and Hatch, C. D.: Instrumentation and measurement

1290 strategy for the NOAA SENEX aircraft campaign as part of the Southeast Atmosphere Study
1291 2013, Atmos. Meas. Tech., 9, 3063-3093, 10.5194/amt-9-3063-2016, 2016.

1292 Wilson, J. C., Lafleu, B. G., Hilbert, H., Seebaugh, W. R., Fox, J., Gesler, D. W., Brock, C. A.,
1293 Huebert, B. J., and Mullen, J.: Function and Performance of a Low Turbulence Inlet for
1294 Sampling Supermicron Particles from Aircraft Platforms, Aerosol Science and Technology, 38,
1295 790-802, 10.1080/027868290500841, 2004.

1296 Worton, D. R., Surratt, J. D., LaFranchi, B. W., Chan, A. W. H., Zhao, Y., Weber, R. J., Park, J.-
1297 H., Gilman, J. B., de Gouw, J., Park, C., Schade, G., Beaver, M., Clair, J. M. S., Crounse, J.,
1298 Wennberg, P., Wolfe, G. M., Harrold, S., Thornton, J. A., Farmer, D. K., Docherty, K. S.,
1299 Cubison, M. J., Jimenez, J.-L., Frossard, A. A., Russell, L. M., Kristensen, K., Glasius, M., Mao,
1300 J., Ren, X., Brune, W., Browne, E. C., Pusede, S. E., Cohen, R. C., Seinfeld, J. H., and
1301 Goldstein, A. H.: Observational Insights into Aerosol Formation from Isoprene, Environmental
1302 Science & Technology, 47, 11403-11413, 10.1021/es4011064, 2013.

1303 Xie, Y., Paulot, F., Carter, W. P. L., Nolte, C. G., Luecken, D. J., Hutzell, W. T., Wennberg, P.
1304 O., Cohen, R. C., and Pinder, R. W.: Understanding the impact of recent advances in isoprene
1305 photooxidation on simulations of regional air quality, Atmos. Chem. Phys., 13, 8439-8455,
1306 10.5194/acp-13-8439-2013, 2013.

1307 Xu, L., Suresh, S., Guo, H., Weber, R. J., and Ng, N. L.: Aerosol characterization over the
1308 southeastern United States using high-resolution aerosol mass spectrometry: spatial and
1309 seasonal variation of aerosol composition and sources with a focus on organic nitrates, Atmos.
1310 Chem. Phys., 15, 7307-7336, 10.5194/acp-15-7307-2015, 2015.

1311 Zhang, H., Yee, L. D., Lee, B. H., Curtis, M. P., Worton, D. R., Isaacman-VanWertz, G.,
1312 Offenberg, J. H., Lewandowski, M., Kleindienst, T. E., Beaver, M. R., Holder, A. L., Lonneman,
1313 W. A., Docherty, K. S., Jaoui, M., Pye, H. O. T., Hu, W., Day, D. A., Campuzano-Jost, P.,
1314 Jimenez, J. L., Guo, H., Weber, R. J., de Gouw, J., Koss, A. R., Edgerton, E. S., Brune, W.,
1315 Mohr, C., Lopez-Hilfiker, F. D., Lutz, A., Kreisberg, N. M., Spielman, S. R., Hering, S. V., Wilson,
1316 K. R., Thornton, J. A., and Goldstein, A. H.: Monoterpenes are the largest source of
1317 summertime organic aerosol in the southeastern United States, Proceedings of the National
1318 Academy of Sciences, 115, 2038, 2018.

1319 Zhang, Q., Stanier, C. O., Canagaratna, M. R., Jayne, J. T., Worsnop, D. R., Pandis, S. N., and
1320 Jimenez, J. L.: Insights into the Chemistry of New Particle Formation and Growth Events in
1321 Pittsburgh Based on Aerosol Mass Spectrometry, Environmental Science & Technology, 38,
1322 4797-4809, 10.1021/es035417u, 2004.

1323 Zhang, Q., Alfarra, M. R., Worsnop, D. R., Allan, J. D., Coe, H., Canagaratna, M. R., and
1324 Jimenez, J. L.: Deconvolution and Quantification of Hydrocarbon-like and Oxygenated Organic
1325 Aerosols Based on Aerosol Mass Spectrometry, Environmental Science & Technology, 39,
1326 4938-4952, 2005.

1327 Zhang, Q., Jimenez, J. L., Canagaratna, M. R., Allan, J. D., Coe, H., Ulbrich, I., Alfarra, M. R.,
1328 Takami, A., Middlebrook, A. M., Sun, Y. L., Dzepina, K., Dunlea, E., Docherty, K., DeCarlo, P.
1329 F., Salcedo, D., Onasch, T., Jayne, J. T., Miyoshi, T., Shimono, A., Hatakeyama, S., Takegawa,
1330 N., Kondo, Y., Schneider, J., Drewnick, F., Borrmann, S., Weimer, S., Demerjian, K., Williams,
1331 P., Bower, K., Bahreini, R., Cottrell, L., Griffin, R. J., Rautiainen, J., Sun, J. Y., Zhang, Y. M.,
1332 and Worsnop, D. R.: Ubiquity and dominance of oxygenated species in organic aerosols in
1333 anthropogenically-influenced Northern Hemisphere midlatitudes, Geophysical Research Letters,
1334 34, L13801, 2007.

Zheng, Y., Unger, N., Hodzic, A., Emmons, L., Knote, C., Tilmes, S., Lamarque, J. F., and Yu, P.: Limited effect of anthropogenic nitrogen oxides on secondary organic aerosol formation, Atmos. Chem. Phys., 15, 13487-13506, 10.5194/acp-15-13487-2015, 2015.

Supplemental Information

In the main text, we noted a discrepancy between overall average aerosol volume estimates based on size measurements vs. AMS for the flight analyzed here (see Figure S1). We checked to see if this bias was also present in the individual plumes studied here by calculating the volume changes from the sizing instruments and the derived volume changes from the AMS+rBC mass. There is quite a bit of scatter in the volume enhancements, with with some of the points falling along the same line as the data for this flight and some falling significantly below the line. It is unclear why the two types of volume measurements disagree more for this flight. Therefore, the bias in volume changes introduces additional uncertainty in the magnitude of the plume enhancements, which is not included in the uncertainty propopagation.

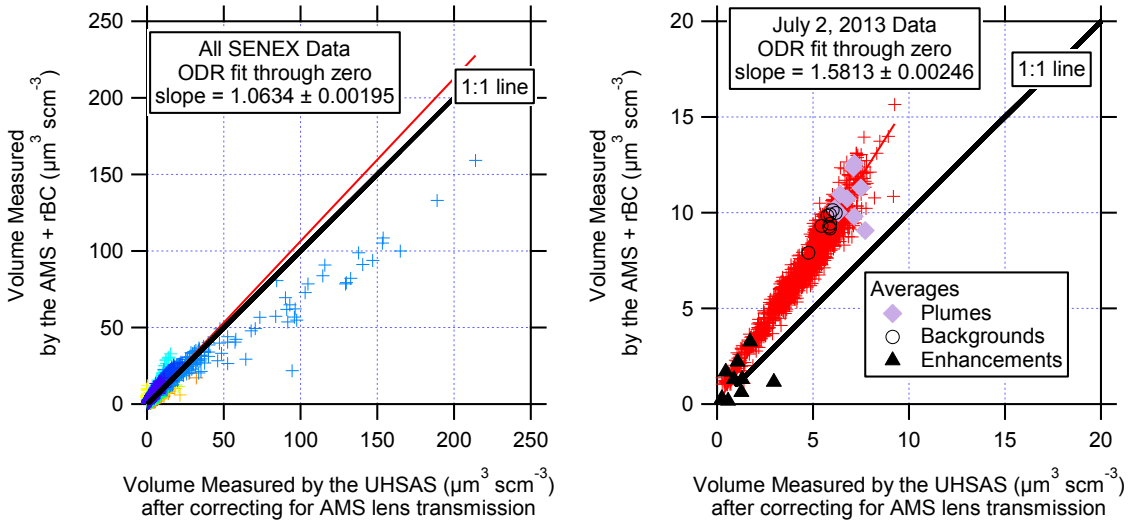

Figure S1. Aerosol volume measured using the total aerosol mass from the AMS plus refractory black carbon (rBC) and mass-weighted densities versus the aerosol volume measured by optical size with the UHSAS after correcting for AMS lens transmission. The procedure for calculating the mass-weighted density is described by Bahreini et al. (2009). On average, the measured aerosol volume from composition is roughly equal to the measured aerosol volume from size for the entire SENEX study (left hand panel) and is higher than one for the flight analyzed here (July 2, 2013, right hand panel).

Corrections for AMS UMR nitrate data and applicability to $pRONO_2$ estimation

Nitrate in the AMS is quantified in unit mass resolution mode (UMR) as the sum of the estimated NO^+ at *m/z* 30 and NO_2^+ at *m/z* 46, with a correction factor to account for the smaller ions (N^+ and HNO_3^+, mostly) produced from nitrate (Allan et al., 2004b). The default AMS UMR quantification algorithm (documented in the AMS "fragmentation table") estimates NO^+ as the total signal at *m/z* 30 minus a small (2.2% of OA at *m/z* 29, "Org29" in AMS parlance) subtraction to account for organic interferences and an isotopic correction for naturally-occurring $^{15}N_2$ from nitrogen in air. The default UMR fragmentation table was developed for mixed ambient aerosols, in particular in urban studies, and it is the responsibility of each AMS user to correct it as needed for each study. In environments with high biogenic contributions to total OA, and/or

low total nitrate concentrations, the contribution of the CH_2O^+ ion can be much larger than the default subtraction at *m/z* 30. Similarly, the $CH_2O_2^+$ ion at *m/z* 46 becomes non-negligible, and hence nitrate reported from AMS data with UMR resolution will frequently be overestimated in these situations. The poor performance of the default AMS correction is likely due to the initial focus on urban OA with high nitrate fractions when deriving those corrections (Allan et al., 2004b;Zhang et al., 2004).

Here we derive a set of corrections based on an aircraft high-resolution (HR) dataset acquired with the University of Colorado HR-AMS (Dunlea et al., 2009) on the NASA DC-8 during the SEAC^{4}RS campaign (Toon et al., 2016). SEAC^{4}RS took place with a strong emphasis on the SEUS 6 weeks after the SENEX flight analyzed in this manuscript. Based on an initial screening of the correlations of the CH_2O^+ and $CH_2O_2^+$ ions with UMR signals, 10 potential UMR *m/z* between *m/z* 29 and *m/z* 53 were selected as viable for deriving suitable corrections. Further analysis using three specific SEAC^{4}RS flights (RF11 on 30 Aug 30th, 2013, RF16 on Sep 11th, 2013 and RF18 on Sep 16th, 2013) that covered a wide range of OA composition with both strong biogenic contributions and fresh and aged biomass plumes showed that only four *m/z* (29, 42, 43 and 45) had good enough S/N and robust enough correlations to be used as corrections. Table S1 summarizes the correction coefficients obtained in this analysis, and Figure S2 shows the ability of matching the actual NO^+ and NO_2^+ signals (as obtained from high-resolution analysis of these flights) with the corrected UMR procedure. These corrections are applied as:

$$\text{UMR NO} = \text{Signal}(m/z30) - a_i * \text{Signal}(\text{Variable}_i)$$
$$\text{UMR NO}_2 = \text{Signal}(m/z\ 46) - b_i * \text{Signal}(\text{Variable}_i)$$

with the coefficients a_i and b_i as reported in Table S1. It should be noted that in all cases the contributions of $C^{18}O^+$ to *m/z* 30 need to be subtracted first before applying the correction (which is constrained to the organic CO_2^+ signal, measured at *m/z* 44, by the naturally-occurring isotopic ratio and assuming that OA produces $CO^+ = CO_2^+$ (Zhang et al., 2005;Takegawa et al., 2007). Likewise, the contribution of $^{13}CO^+$ to Org29 needs to be subtracted first. It is hence very important for this analysis that the corrections to the AMS frag table to suitably estimate the contribution of gas phase CO_2^+ to total *UMR m/z* 44 as well as the baseline correction for *m/z* 29 be properly applied first (Allan et al., 2004b). Finally, also note that the corrections using *m/z* 29 and 43 are rather based on Org29 and Org43, which are standard AMS products that take the OA relative ionization efficiency (RIE) into account.

For the SEAC^{4}RS dataset, the corrections amounted to on average subtracting 55% from UMR *m/z* 30 and 33% from UMR *m/z* 46. Despite this large subtraction, the corrected data correlates very well with the HR AMS results, with less than 5% deviation in the regression slope between the two datasets.

Although all of the corrections in Table S1 were valid for the SEAC^{4}RS data set, for the flight analyzed here we chose Org29 to correct *m/z* 30 and *mz* 45 correction to correct *m/z* 46 because they were the closest organic signals to the UMR nitrate peaks with organic

interferences and may be more valid for other field studies where different types of OA are sampled. After these UMR signals were corrected and the appropriate RIEs and CE were applied, the nitrate mass concentrations in the final data archive for the flight analyzed here were reduced by 0-0.24 μg sm^{-3}, averaging 0.11 μg sm^{-3} or 32%. The corresponding increase in OA due to the organic interferences in the UMR nitrate had linear dependence on the reported OA mass concentrations (r^2 = 0.89) with a slope of 1.3%.

To estimate the fraction of nitrate that is organic nitrate ($pRONO_2$) the use of the NO_2^+/NO^+ ratio with an empirically determined $pRONO_2$ calibration ratio has been successfully used previously with HR-AMS data (Farmer et al., 2010;Fry et al., 2013;Ayres et al., 2015;Fisher et al., 2016;Day et al., 2017;Palm et al., 2017;Lee et al., 2016). Figure S2 summarizes how well the ratio of the corrected UMR *m/z* 30 and 46 signals correlate with the NO_2^+ and NO^+ (and ratios) determined using HR data. As expected, there is considerable scatter at very low nitrate concentrations (which is a considerable part of the dataset, as the time series shows, since the free troposphere was sampled extensively). However, for the predicted $pRONO_2$ (which is mass-weighted), most of this scatter disappears, and for concentrations above 0.1 μg sm^{-3} of nitrate there is good agreement between the HR results and the UMR-corrected $pRONO_2$, regardless of the correction chosen. For lower concentrations the scatter is considerable larger, with the Org29 correction providing the best overall agreement. Based on the variability in this dataset for this correction (Org29), we estimate the uncertainty in $pRONO_2$ fraction apportionment using UMR to be about 30%, in addition to an estimated uncertainty for the apportionment method using HR of 20%. From the comparison of UMR-corrected total nitrate to HR nitrate (not shown), we estimate an additional error of 5% for total nitrate error using these corrections.

As mentioned in the main text, the empirically determined $pRONO_2$ calibration ratio used for the flight data analyzed here was the ratio of NO_2^+/NO^+ from the ammonium nitrate calibration aerosols divided by 2.8. This factor was determined as the average of several literature studies (Fry et al., 2009;Farmer et al., 2010;Rollins et al., 2009;Sato et al., 2010;Fry et al., 2011;Boyd et al., 2015) and applied according to the “ratio of ratios” method (Fry et al., 2013). The ammonium nitrate NO_2^+/NO^+ ratio was obtained from the two calibrations on 30 June and 7 July that bracketed the flight on 2 July, as described above. This ratio averaged 0.490. Hence, the organic nitrate NO_2^+/NO^+ ratio was estimated to be 0.175. The ratio of NO_2^+/NO^+ from the flight data was then used with the $pRONO_2$ and ammonium nitrate NO_2^+/NO^+ calibration ratios to estimate the fraction of the total corrected nitrate mass concentrations that was organic ($pRONO_2$) or inorganic (nitrate associated with ammonium or NH_4NO_3). Propagating the 30% UMR vs HR uncertainty and 20% apportionment (see above) error on top of the 34% AMS total nitrate measurement uncertainty results in ±50% uncertainties in the derived organic nitrate mass concentrations (and similar for NH_4NO_3; however it will depend on the relative contributions of $pRONO_2$ and NH_4NO_3 to total nitrate since the absolute concentration errors associated with $pRONO_2$ - NH_4NO_3 apportionment should be similar [64]).

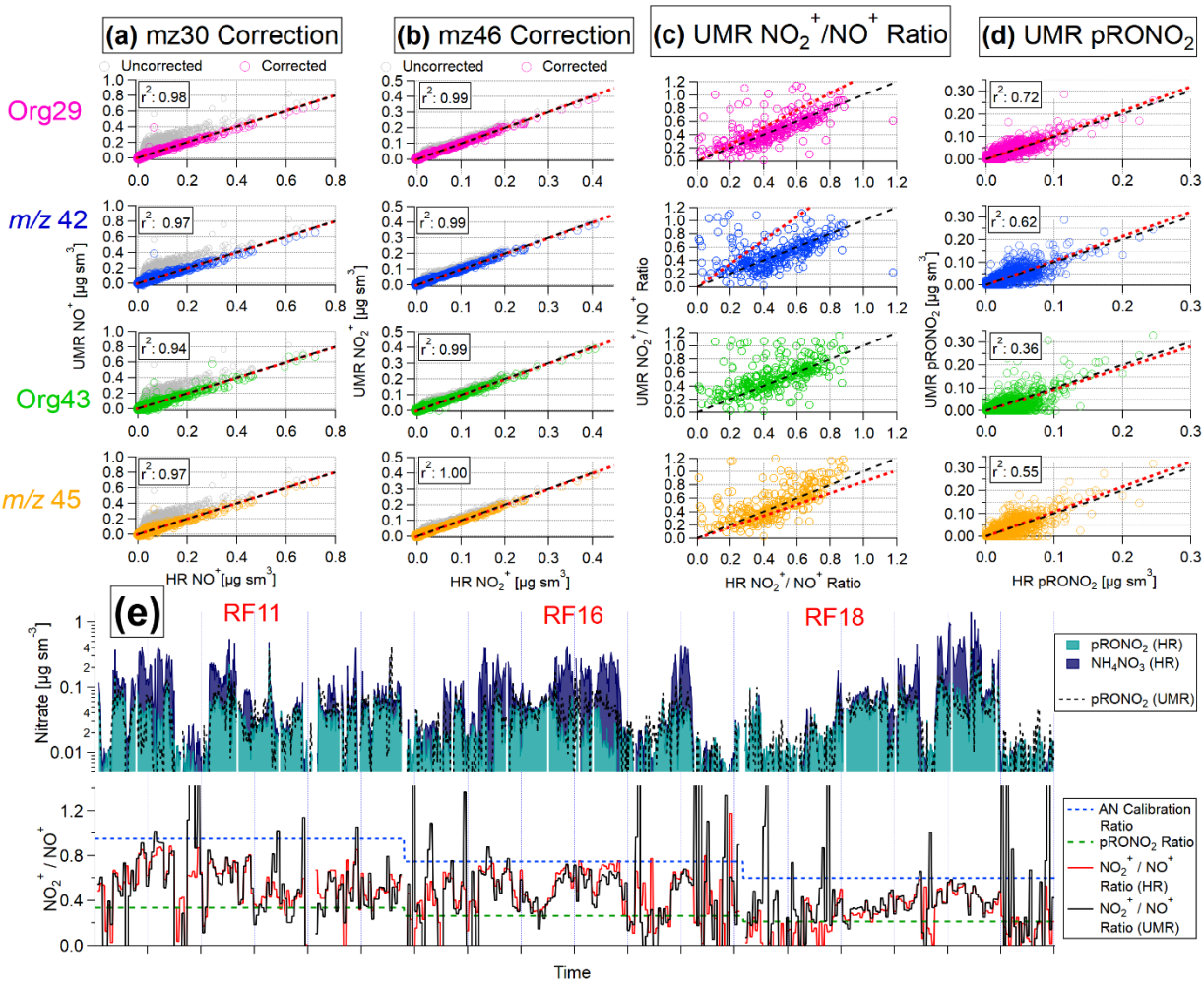

Figure S2. (a and b) Comparison of *m/z* 30 and 46 with the NO^+ and NO_2^+ signals from the high resolution analysis of the AMS data before and after applying the four different corrections listed in Table S1. The Pearson r^2 for the corrected dataset is shown as well. (c) Comparison of the NO_2^+/ NO^+ ratio obtained from HR analysis with the ratios of the corrected UMR NO and NO_2 variables (d) Comparison of the $pRONO_2$ concentrations derived using the HR and UMR NO_2^+/ NO^+ ratios. (e) Time series of the total and speciated nitrate as reported from HR analysis of the SEAC[4]RS data (DOI: 10.5067/Aircraft/SEAC4RS/Aerosol-TraceGas-Cloud) compared to the speciation using the Org29 correction (note the logarithmic scale). The bottom time series shows the NO_2^+/ NO^+ ratio that the speciation is based on, again for the HR and corrected UMR case.

Table S1. Coefficients used to correct *m/z* 30 and 46 to estimate total nitrate.

AMS Variable	Correction coefficient for *m/z* 30 (a_i)	Correction coefficient for *m/z* 46 (b_i)
Org29	0.215	0.037
m/z 42	0.51	0.092
Org43	0.215	0.037
m/z 45	0.72	0.127

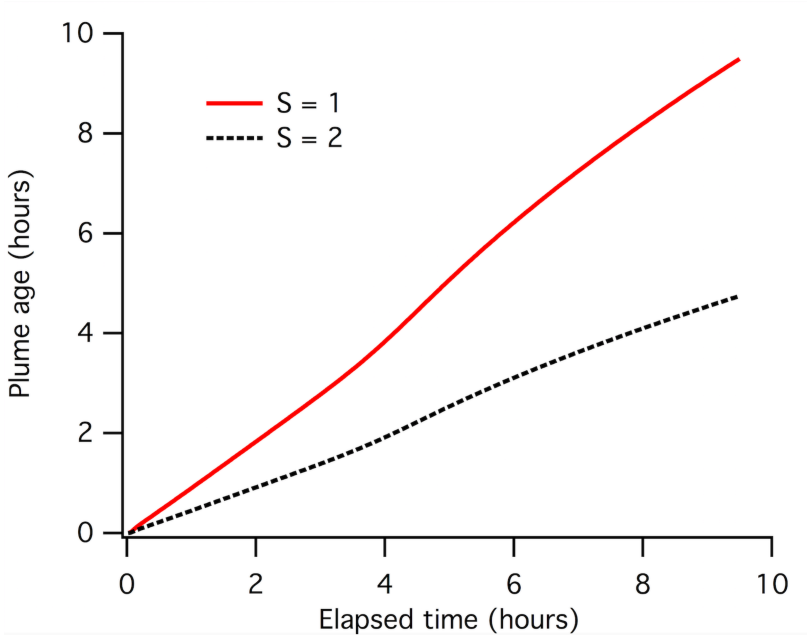

Figure S3. Calculated plume age vs. elapsed time in a box model run for a single representative night. Plume ages on the y-axis are calculated based on Equation 1 in the main text but using model NO_2 and O_3 data. Time since sunset on the x-axis is the model elapsed time (i.e., run time of the model during darkness).

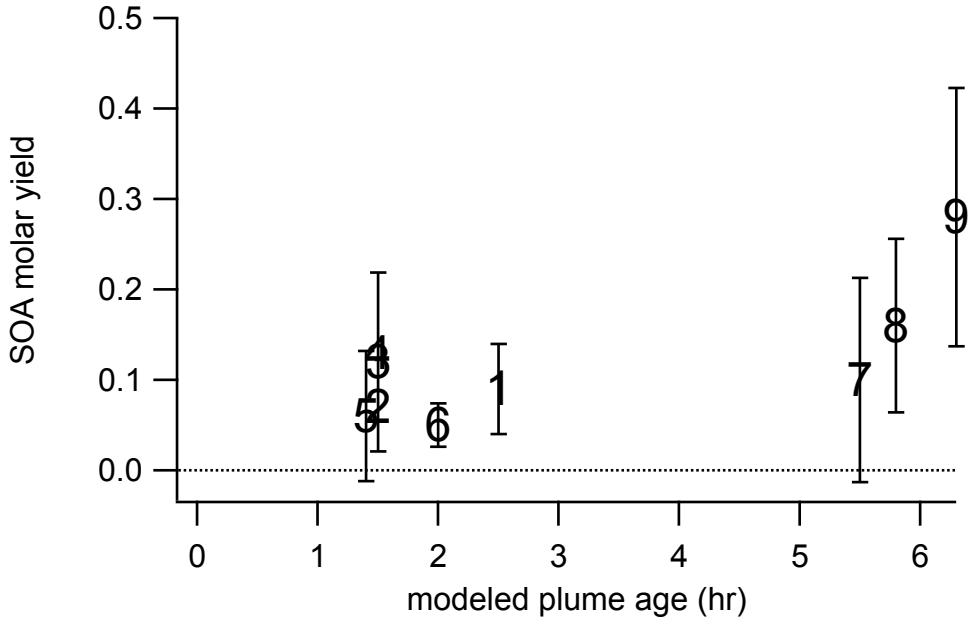

Figure S4. SOA molar yield is positively correlated with estimated plume age. This SOA molar yield is based on Eq. 3, with error bars determined by propagation of observed variability in $pRONO_2$ and isoprene, where multiple point averaging was possible. Markers correspond to

plume numbers.). Based on the box model described in more detail below, the first-generation isoprene products peak at a approximately 4 hours plume age and then begin to decay.

Table S2. Peak ambient (wet) aerosol surface area during each plume used in the yield analysis (plume numbers 1 – 9), and for the two longer urban plumes transected at the end of the flight.

plume number	7/2/13 plume time (UTC)	Peak aerosol surface area ($\mu m^2\ cm^{-3}$)
1	2:18	280
2	2:20	370
3	2:21	470
4	3:03	340
5	3:55	800
6	4:34	470
7	4:37	370
8	4:39	420
9	5:04	490
Urban plume	5:36	340
Urban plume	6:37	300

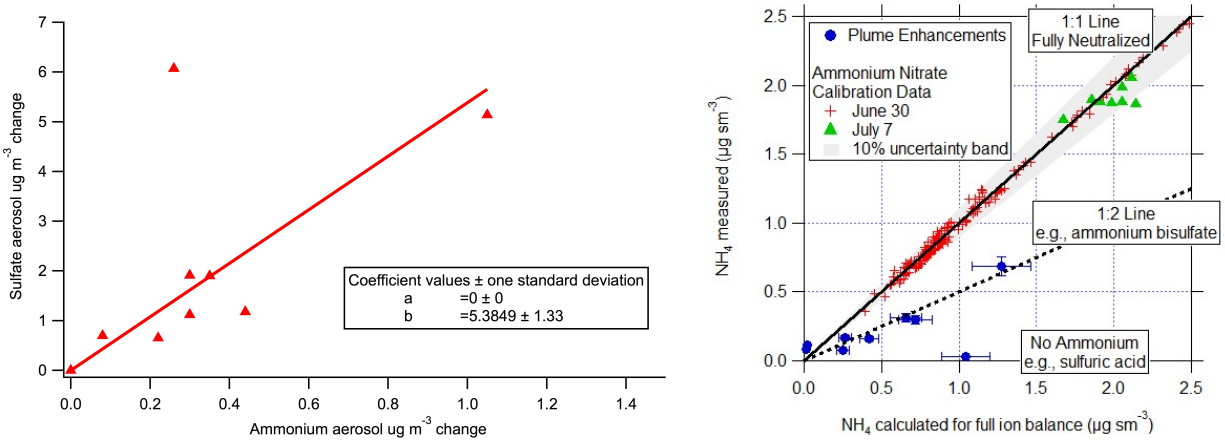

Figure S5. (a) In-plume change in sulfate mass concentration vs. change in ammonium aerosol mass concentration is generally well correlated, with a slope of 5.4. The masses of the cations and anions would give an ion balance for pure $(NH_4)_2SO_4$ of $MW(SO_4)/(2 \times MW(NH_4)) = 2.7$, and for $(NH_4)HSO_4$ of $MW(SO_4)/(MW(NH_4)) = 5.4$. Hence, this slope provides support for a mix of these two ammonium sulfate salts, with sometimes exclusively $(NH_4)HSO_4$. This is consistent with incomplete neutralization of the sulfate mass by ammonium. The one clear outlier (sulfate increase of 6 µg m^{-3} for Plume #5) suggests excess sulfate, rendering ammonium or other inorganic nitrate formation even less likely. Points with ammonium aerosol below 0.1 µg m^{-3} are within the variability of that measurement; their omission does not change the slope. (b) Measured vs. calculated (ion balanced) NH_4 for calibration data and plume enhancements. This also shows that plumes are acidic than ammonium sulfate, ruling out the possibility of inorganic nitrate formation.

Additional AMS and auxiliary data from plumes

Table S3. Additional information for the list of plumes used in this NO_3 + isoprene SOA yield analysis, for which key yield-related data is presented in Table 1. For each plume, the delta-values listed indicate the difference between in-plume and outside-plume background in average observed concentration. After each plume number, the numbers of points averaged for isoprene and AMS, respectively, are listed. Plume numbers annotated with * indicate brief plumes for which only single-point measurements of in-plume aerosol composition were possible. Also shown are the plume changes in isoprene used in the present analysis (Δisop, the difference between in-plume and background isoprene concentration, reproduced from Table 1), alongside for comparison the Δisop determined as the difference between in-plume isoprene and the modeled sunset (initial) concentration of isoprene present at that location outside of the plume, determined using an iterative box model (Edwards et al., 2017). The similarity between these two values for most points suggests that the isoprene just outside of each plume transect was largely unperturbed from the sunset initial value.

plume number [#isop/#AMS]	**7/2/13 plume time (UTC)**	**ΔORG_{aero} ($\mu g\ m^{-3}$)**	**$\Delta NH_{4,aero}$ ($\mu g\ m^{-3}$)**	**$\Delta SO_{4,aero}$ ($\mu g\ m^{-3}$)**	**Temp (C)**	**%RH**	**Δisop (pptv)**	**Δisop from model (pptv)**	**Isop:MT Mole Rat**
Typical variability ($\mu g\ m^{-3}$):		0.75	0.1	0.5					
1 [2/3]	2:18	0.35	0	0	23.6	66.5	-335	-327	36.5
2 [*]	2:20	0.89	0.3	1.91	23.6	65	-404	-453	71.4
3 [4/5]	2:21	1.25	1.05	5.14	23.6	65.2	-228	-337	16.6
4 [*]	3:03	0.16	0.08	0.7	21.2	68.1	-453	-391	50.6
5 [3/4]	3:55	0.32	0.26	6.07	21.9	65.5	-255	-376	34.2
6 [2/2]	4:34	0.57	0.3	1.12	19.9	74.6	-713	-233	17.3
7 [5/6]	4:37	1.05	0.22	0.65	19.7	76.2	-298	-221	14.2
8 [2/3]	4:39	1.26	0.44	1.18	18.3	82.2	-443	-353	11.0
9 [7/8]	5:04	1.45	0.35	1.9	17.2	84.8	-293	-434	17.8

Box model calculations

Box model simulations were performed using the Dynamically Simple Model of Atmospheric Chemical Complexity (DSMACC, http://wiki.seas.harvard.edu/geos-chem/index.php/DSMACC_chemical_box_model), containing the Master Chemical Mechanism v3.3.1 chemistry scheme (http://mcm.leeds.ac.uk/MCM/). The model approach is similar to that described in detail in Edwards et al. 2017, and the accompanying supplement, with the model run over a 9.5 hour night to simulate the nocturnal residual layer. For the nocturnal simulation used in this work (for both the plume lifetime calculation and the peroxy radical lifetime analysis in Sect. 4.3) the model was initialized with concentrations of the constraining species representative of the SENEX observations (Table S4). As the model is simulating power plant plume evolution from point of emission, a starting NO mixing ratio of 10 ppb was used to constrain NO_x, and the chemistry scheme was subsequently allowed to partition the reactive nitrogen. The top panels in Figure S7 show the evolution of key species during this nocturnal simulation.

Table S4: Species constrained (MCM v3.3.1 names) during model simulations and constraining values. Constraint column indicates if species concentrations were held at the constrained value throughout the simulation (Fixed) or allowed to vary after initialization (Initial).

Species	Mixing ratio	Units	Constraint
NO	9.28	ppb	Initial
O3	55.72	ppb	Initial
CO	134.00	ppb	Fixed
CH4	1920.00	ppb	Fixed
C5H8	2606.80	ppt	Initial
APINENE	38.87	ppt	Initial
BPINENE	195.50	ppt	Initial
LIMONENE	12.42	ppt	Initial
MACR	454.13	ppt	Initial
MVK	1006.00	ppt	Initial
IC4H10	47.00	ppt	Fixed
NC4H10	128.00	ppt	Fixed
C2H6	1199.00	ppt	Fixed
C2H4	117.00	ppt	Fixed
C2H2	145.00	ppt	Fixed
NC6H14	20.00	ppt	Fixed
IC5H12	120.00	ppt	Fixed
NC5H12	76.00	ppt	Fixed
C3H8	344.00	ppt	Fixed
C3H6	26.00	ppt	Fixed
CH3COCH3	2556.00	ppt	Fixed
BENZENE	35.90	ppt	Fixed
C2H5OH	2239.00	ppt	Fixed
MEK	309.00	ppt	Fixed
CH3OH	5560.00	ppt	Fixed

The daytime simulation used for comparison in Sect. 4.3 of the main manuscript (lower panels of Figure S7) uses the same initialization as the nocturnal simulation; with the only difference being the model is run during the daytime. Photolysis rates are calculated using TUV (https://www2.acom.ucar.edu/modeling/tropospheric-ultraviolet-and-visible-tuv-radiation-model). The daytime simulation does not accurately simulate daytime mixing ratios of species such as O_3 representative of SENEX observations. However, the intent of this simulation is to compare model daytime peroxy radical fate and lifetime with the nocturnal simulation. The presence of

intense convective mixing in the daytime planetary boundary layer of the Southeast US makes accurately modeling these concentrations difficult with a zero dimensional model.

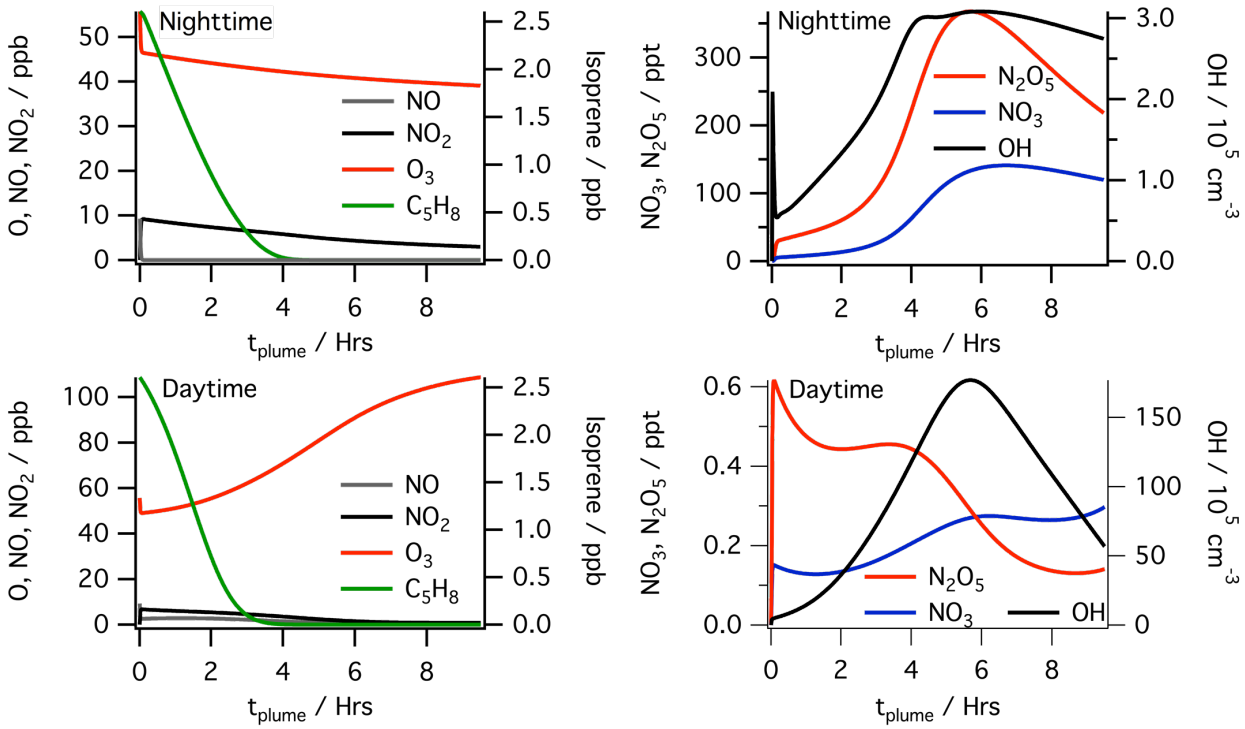

Fig. S6. Model calculated NO, NO_2, O_3, and isoprene (left) and NO_3, N_2O_5 and OH (right for the nocturnal (top) and daytime (bottom) simulations shown in Sect. 4.3.

Additional considerations investigated via RO_2 fate box modeling

Based on the potentially larger than previously estimated contribution of RO_2+RO_2 reactions at night, we considered a related possible source of a high bias in the determined SOA yields. If NO_3 reaction with the major daytime isoprene oxidation products MVK and/or MACR produces RO_2 radicals that can cross-react with NO_3 + isoprene products to produce condensable products, this would be a mechanism of recruiting isoprene-derived organic mass into the aerosol, but that original isoprene oxidation would not be counted in the denominator of the yield calculation, since its interaction with NO_3 began as MACR or MVK. In the box model, substantial MVK and MACR are available in the plume at nighttime, but only MACR reacts with NO_3, and a maximum fraction of one-quarter of MVK+MACR losses go to reaction with NO_3 overnight (see Figure S8). In addition, in our power plant plume observations, MVK+MACR are not observed to be appreciably depleted by the large NO_3 injection, further suggesting that this chemistry is not a substantial additional source of SOA (see Figure S9).

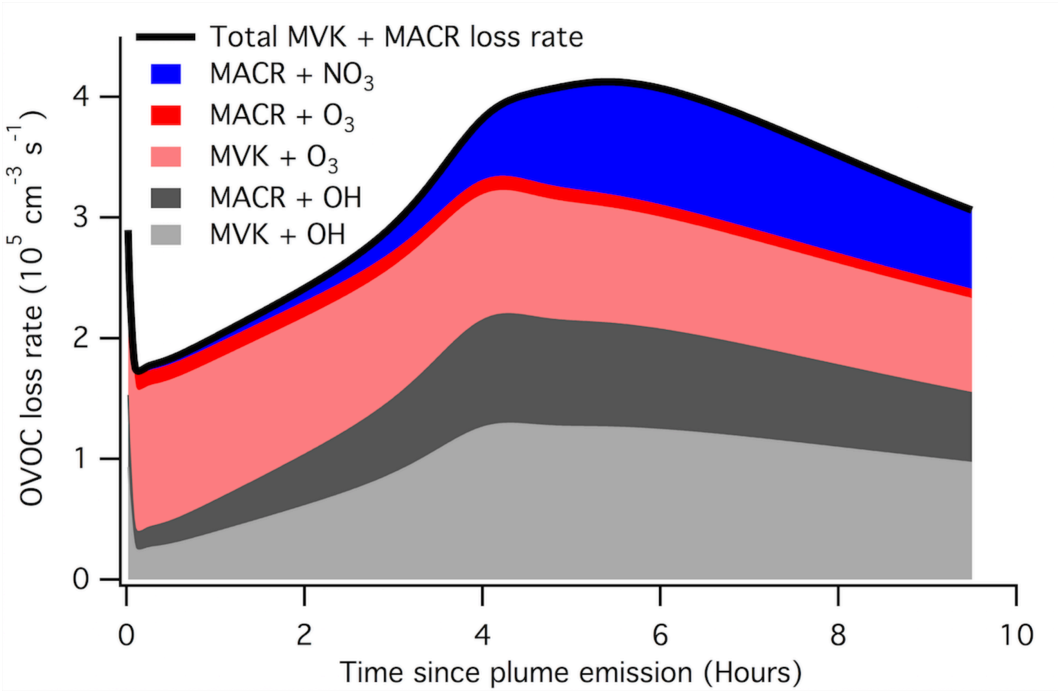

Figure S7. Calculated (via MCM) loss rate contributions for the daytime isoprene products methyl vinyl ketone (MVK) and methacrolein (MACR) in the simulated nighttime plume used in the text. Only MACR reacts with NO_3, and the contribution of this process to total losses (green stack) is relatively minor.

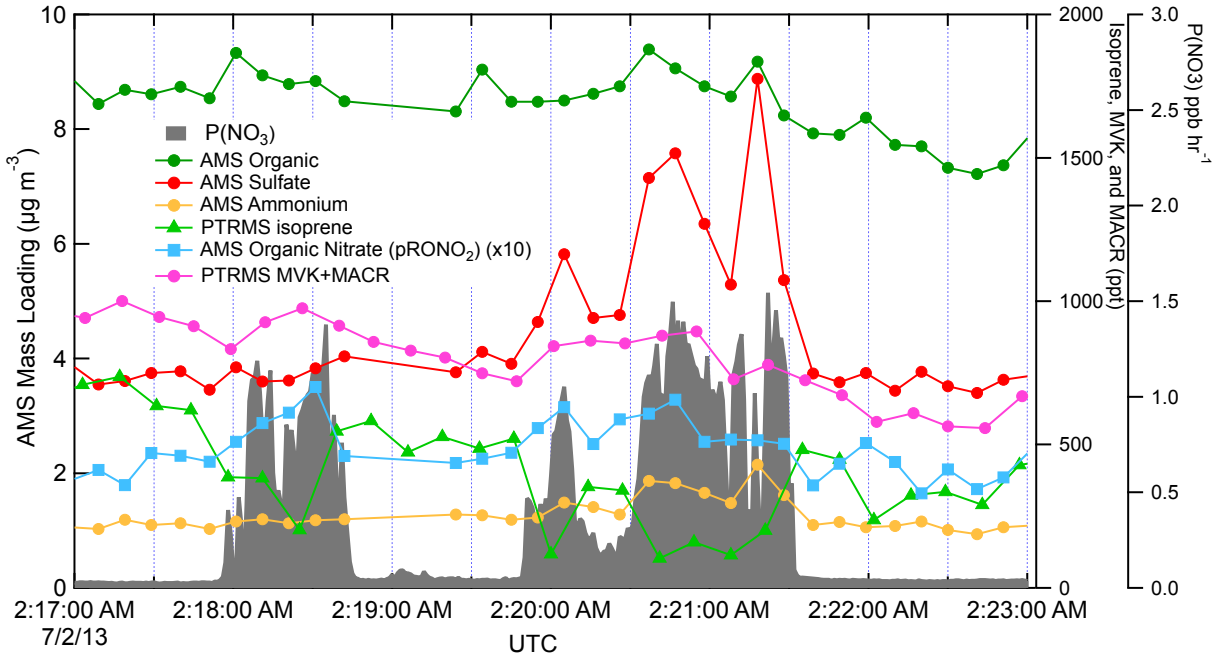

Figure S8. MVK and MACR are not titrated on the timescale of these yield estimates in power plant plumes.

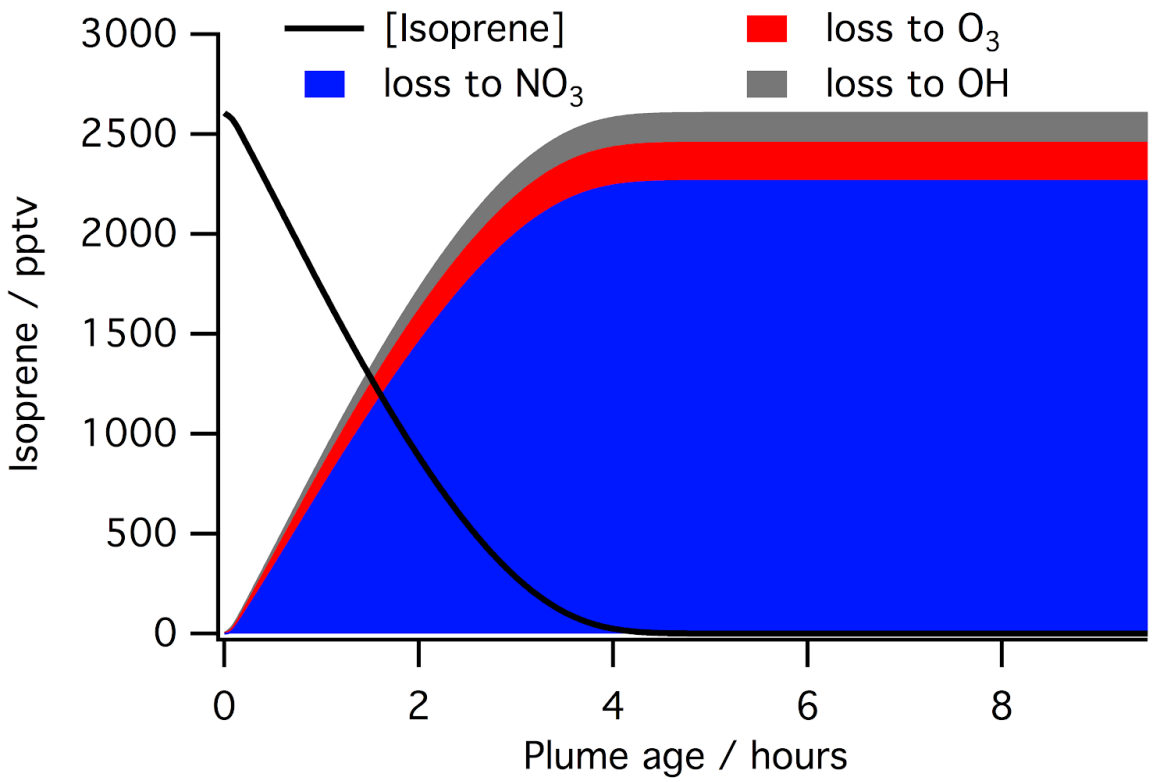

Figure S9. Model simulation of typical in-plume consumption of isoprene (black line), and stacked plot showing the contributions to this from the NO_3, O_3, and OH. Modeled plume was emitted at sunset, so this represents nocturnal processing under power plant plume conditions.

Two urban plume case studies

In addition to the nine power plant plumes analyzed above to determine the NO_3 + isoprene SOA molar yield, towards the end of the July 2 flight, the Birmingham urban plume was intercepted twice (around 5:36 am and 6:37 am UTC, Fig. 8). These downwind urban plumes are among the most aged plumes (estimated at 5.2 and 5.8 hours, respectively), but are also substantially more diffuse than the narrow power plant plume intercepts and have lower peak $P(NO_3)$. Nevertheless, we note that these two plumes contain periods of apparent anti-correlation of isoprene and organic nitrate aerosol time series and high apparent SOA molar yields (23%, 19%) and mass yields (62%, 51%), if calculated by the same method as above and omitting the period of vertical profiling in the second plume. Potentially complicating these urban SOA yield determinations is the fact that the inorganic fraction of nitrate was much larger than in the power plant plumes (see Fig. 8). The background isoprene is also somewhat lower in these urban plumes, potentially shifting the NO_3/N_2O_5 fate to reactions other than NO_3 + isoprene (see Fig. S4 in Edwards et al. (Edwards et al., 2017)). The aerosol surface area is not noticeably higher in these urban plumes, which one might expect to lead to a larger contribution of N_2O_5 uptake and hydrolysis. In the more complex mix of gases characteristic of an urban plume, we hesitate to attribute these apparent yields exclusively to the NO_3 + isoprene reaction.

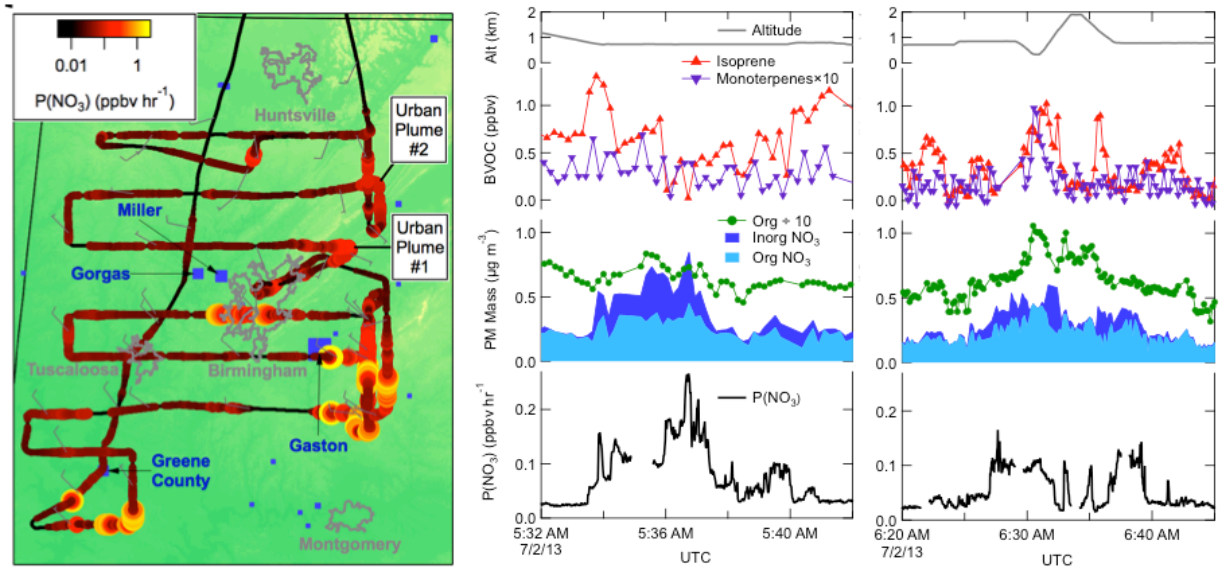

Figure S10. Flight map and time series of two urban plume intercepts, showing anticorrelation of organic nitrate and isoprene. These more diffuse plumes, with lower $P(NO_3)$ and larger inorganic nitrate contribution, make yield determination more uncertain, so we do not include them in the overall yield determination. However, using the same methodology as for the power plant plumes would give similarly high yields for these very aged plumes.